U.S. DEPARTMENT OF ENERGY

PNNL-22549

Prepared for the U.S. Department of Energy
under Contract DE-AC05-76RL01830

Pellet-Cladding Mechanical Interaction Failure Threshold for Reactivity Initiated Accidents for Pressurized Water Reactors and Boiling Water Reactors

CE Beyer
KJ Geelhood

June 2013

Pacific Northwest
NATIONAL LABORATORY

Proudly Operated by Battelle Since 1965

DISCLAIMER

PACIFIC NORTHWEST NATIONAL LABORATORY
operated by
BATTELLE
for the
UNITED STATES DEPARTMENT OF ENERGY
under Contract DE-AC05-76RL01830

Printed in the United States of America

Available to DOE and DOE contractors from the
Office of Scientific and Technical Information,
P.O. Box 62, Oak Ridge, TN 37831-0062;
ph: (865) 576-8401
fax: (865) 576-5728
email: reports@adonis.osti.gov

Available to the public from the National Technical Information Service
5301 Shawnee Rd., Alexandria, VA 22312
ph: (800) 553-NTIS (6847)
email: orders@ntis.gov <http://www.ntis.gov/about/form.aspx>
Online ordering: http://www.ntis.gov

(8/2010)

PNNL-22549

Pellet-Cladding Mechanical Interaction Failure Threshold for Reactivity Initiated Accidents for Pressurized Water Reactors and Boiling Water Reactors

CE Beyer
KJ Geelhood

June 2013

Prepared for
the U.S. Department of Energy
under Contract DE-AC05-76RL01830

Pacific Northwest National Laboratory
Richland, Washington 99352

Summary

Pacific Northwest National Laboratory (PNNL) has been requested by the U.S. Nuclear Regulatory Commission to evaluate the reactivity initiated accident (RIA) tests that have recently been performed in the Nuclear Safety Research Reactor (NSRR) and CABRI (French research reactor) on uranium dioxide (UO_2) and mixed uranium and plutonium dioxide (MOX) fuels, and to propose pellet-cladding mechanical interaction (PCMI) failure thresholds for RIA events. This report discusses how PNNL developed PCMI failure thresholds for RIA based on least squares (LSQ) regression fits to the RIA test data from cold-worked stress relief annealed (CWSRA) and recrystallized annealed (RXA) cladding alloys under pressurized water reactor (PWR) hot zero power (HZP) conditions and boiling water reactor (BWR) cold zero power (CZP) conditions.

PNNL has modified the original correlations in "Fuel System Design," Chapter 4, Section 4.2, Appendix B, Revision 3 of *Standard Review Plan for the Review of Safety Analysis Reports for Nuclear Power Plants LWR Edition* (NRC 2007) as follows:

1. The PWR correlation for CWSRA has been changed to be a function of excess hydrogen rather than oxide-to-wall ratio.
2. PNNL developed a correlation for PWR RXA alloys at HZP conditions by adjusting the original BWR correlation for RXA cladding up by 18 cal/g (cold-to-hot adjustment) except for the 150 cal/g portion for ballooning and rupture. This adjustment allows the Standard Review Plan BWR correlation for CZP with RXA cladding to be applied to PWRs with RXA cladding at HZP.
3. PNNL developed a correlation for BWR CWSRA alloys at CZP by adjusting the original PWR correlation for CWSRA cladding down by 18 cal/g (hot-to-cold adjustment), except for the 150 cal/g portion for ballooning and rupture. This adjustment allows the Standard Review Plan PWR correlation for HZP with CWSRA cladding to be applied to BWRs with CWSRA cladding at CZP.

The rodlets tested in CABRI and NSRR criteria are limited with few replicate data and with little or no data at some excess hydrogen levels. This results in considerable uncertainty in the PCMI failure thresholds developed in this report where the data are lacking. Another significant uncertainty in the PWR failure thresholds is related to the cold-to-hot adjustment for CZP data and the BWR hot-to-cold adjustment for HZP data because there are only two pairs of cold-versus-hot data used to estimate this adjustment.

The PCMI failure thresholds developed here are proposed to replace those in Appendix B of SRP 4.2 Revision 3 (NRC 2007) and in NRC 1974, although the latter is still applicable for those things not changed in this document or in NRC 2007. U.S. Nuclear Regulatory Commission staff should decide the level of conservatism required for the PCMI failure thresholds in the final SRP 4.2.

Acronyms and Abbreviations

BIGR	Bystry Impulsny Graphitovy Reaktor (Russian Fast Pulse Graphite Reactor)
BWR	boiling water reactor
CABRI	French research reactor
cal/g	calories per gram
CWSRA	cold-worked stress relief annealed
CZP	cold zero power
DBTT	ductile brittle transition temperature
FRAPTRAN	fuel rod analysis program transient
g/d	gap-to-diameter
HZP	hot zero power
ID	inner diameter
IFBA	integral fuel burnable absorber
IGR	Impulse Graphite Reactor
LSQ	least squares
LWR	light water reactor
MDA	Mitsubishi Developed Alloy
MOX	mixed uranium and plutonium dioxide
NSRR	Nuclear Safety Research Reactor
PCMI	pellet-cladding mechanical interaction
pRXA	partially recrystallized annealed
PWR	pressurized water reactor
RIA	reactivity initiated accident
RXA	recrystallized annealed
SPERT-CDC	Special Power Excursion Reactor Test
SRP	Standard Review Plan
UO_2	uranium dioxide
VVER	Vodo-Vodyanoy Energetichesky Reaktor (Russian pressurized water reactor)

Contents

Figures

Tables

1.0 Introduction

Reactivity initiated accident (RIA) tests on rodlets (cut to size from commercial fuel rods) have been performed in the Nuclear Safety Research Reactor (NSRR) and CABRI (French research reactor) on uranium dioxide (UO_2) and mixed uranium and plutonium dioxide (MOX) fuels. This report develops pellet-cladding mechanical interaction (PCMI) failure thresholds for RIAs for pressurized water reactors (PWRs) and boiling water reactors (BWRs).

This report discusses the data used to develop the PCMI failure thresholds and uncertainties in Section 2, the derivation of the PWR PCMI failure threshold for the cold-worked stress relief annealed (CWSRA) and recrystallized annealed (RXA) cladding types in Section 3, and the derivation of the BWR PCMI failure threshold for the RXA and CWSRA cladding types in Section 4. Besides the thresholds being different for "hot" initial conditions and cold zero power (CZP) they are also different for the different cladding heat treatments, CWSRA and RXA, because the hydride orientations are different for these two heat treatments. Therefore, there are four different failure thresholds: CWSRA "hot" and RXA "hot" for PWRs, and RXA CZP and CWSRA CZP for BWRs. The PWR PCMI threshold will be discussed in terms of the variables examined that could possibly affect this threshold, including hydrogen and corrosion level (the most significant impact on threshold), burnup, fuel type (UO_2 and MOX), cladding type, pulse width, and fuel-clad gap size. Some of these variables are directly measured (e.g., pulse width and corrosion) and others (e.g., hydrogen content) are often inferred.

The PCMI failure thresholds for RIA developed in this report are based on simple linear regression or least squares (LSQ) fits of the data and analyses of data. Statistical methods are best applied to truly random data (e.g., the same RIA test repeated over and over again) or the same RIA test repeated with only one variable changing (e.g., hydrogen content). In practice, the challenge is to demonstrate that the other test variables (e.g., pulse width) either have an effect or have no or little effect on the results).

A second goal of this investigation is to quantify the difference between "cold" and "hot" initial conditions. Essentially all available RIA data were taken under test reactor conditions rather than prototypical pressurized light-water-reactor conditions. Adjusting test reactor data to represent light-water-reactor conditions—developing cold-to-hot adjustment for RIA data—has often employed a fuel performance code. By identifying specific RIA test data, particularly those data in which only "hot" and "cold" initial conditions have changed, it is possible to analyze the temperature effect directly. The results are used to produce failure thresholds described in this paper. These results offer an alternative to fuel code-based methods.

Earlier analyses within the United States (NRC 2004 and Alvis et al. 2010), have used fuel performance codes to assist in developing PCMI failure thresholds for RIA events because of the lack of test data with failures under hot conditions. The PCMI thresholds developed previously reflect the assumptions, biases, and uncertainties in these codes as well as the assumptions made in their code application to develop the thresholds. On the other hand, application of RIA data without a "cold-to-hot" correction is arguably conservative and can be developed without application of a fuel performance code. A review of PCMI failure thresholds proposed internationally has been previously performed by Vitanza and Hrehor (2006), many of these were also based on fuel performance code calculated results or based on the data by conservatively assuming no cold-to-hot adjustment.

The RIA empirical database used to derive the PCMI cladding failure thresholds consists of prompt critical, narrow-pulse power excursion experiments. Therefore, these PCMI cladding failure thresholds may not be directly applicable to 1) non-prompt RIA scenarios (e.g., ejection of partially inserted control rod or low-worth control rod), 2) non-prompt accident overpower scenarios (e.g., PWR main steam line break), or 3) non-prompt anticipated operational occurrence overpower scenarios (e.g., PWR control rod bank withdrawal, BWR turbine trip). Relative to a prompt-critical, narrow-pulse power excursion, the broader power excursion exhibited in these scenarios allows additional time for the cladding temperature (and ductility) to increase such that brittle failure is unlikely.

2.0 Discussion of RIA Test Data

The U.S. commercial nuclear power fleet uses fuel rod cladding composed of both CWSRA and RXA zirconium alloys. The RIA empirical database contains several currently used PWR cladding alloys including Zircaloy-4 CWSRA, ZIRLO™ CWSRA, and M5 RXA cladding as well as BWR Zircaloy-2 RXA (majority of BWR cladding used) and CWSRA cladding. A compilation of the PWR and BWR RIA empirical database is presented in Appendix A and Appendix B, respectively. The compilation includes all of these cladding types with the exception of Zircaloy-2 CWRSA. The database also includes Japanese cladding alloys (e.g., Mitsubishi Developed Alloy [MDA]) but does not include Russian cladding alloys (e.g., E110). None of these foreign alloys are currently used in U.S. commercial reactors. Because of test conditions and other factors, not all of the data will be used to derive failure thresholds. Currently some PWRs also use ZIRLO™ that is partially recrystallized annealed (pRXA), however, no RIA test data exist for this cladding type. Section 3.12 describes the applicability of these failure thresholds to pRXA zirconium cladding.

The primary difference between failure threshold versus hydrogen level for CWSRA and RXA cladding appears to be because of the hydrogen level, orientation, and distribution, and these will be discussed in the following sections. Therefore, if future cladding types have a different hydrogen distribution or orientation, they may have a different failure threshold versus hydrogen level than those developed in this report. For example, if a newly developed RXA cladding no longer has hydrides randomly oriented, but are orientated parallel to the direction of stress, this may increase the failure threshold compared to those RXA cladding types tested to date; however, this cladding would have to be tested in-reactor or out-of-reactor at service conditions similar to those for an RIA event to determine if there is justification for a change in the failure threshold. It should further be noted that hydrogen level is often deduced rather measured, and little is known about hydrogen distribution and orientation when hydrogen level is derived without micrographs.

RIA tests performed in the CABRI sodium loop had an initial coolant temperature of 536°F (280°C), which is approximately equal to initial PWR coolant temperatures at hot zero power (HZP) operating conditions. Hence, these test results are directly applicable to PWR HZP conditions. Application of these test results to “at-power” operating conditions for RIA, where initial coolant and cladding temperatures are higher, is conservative because of a higher intrinsic level of cladding ductility at these higher temperatures.

The early RIA tests performed in the NSRR water loop had an initial coolant temperature of 68°F (20°C), which is approximately equal to initial BWR coolant temperatures at CZP operating conditions; two later NSRR tests (FK10 and FK12) on BWR rodlets were tested with initial coolant temperatures of 80°C and 85°C. Whereas PWRs are required to achieve a relatively high reactor coolant system temperature prior to criticality (reactor coolant pump heat used to heat up coolant), BWRs begin withdrawing control blades and achieve criticality at low temperatures. As a result, the early NSRR test results (including FK10 and FK12) are directly applicable to BWR CZP startup conditions. Similar to above, application of these room-temperature test results to higher-temperature BWR operating conditions is conservative.

Recent RIA tests performed in the NSRR hot capsule had an initial coolant temperature of 509°F to 545°F (265°C to 285°C). These test results will be used to quantify the temperature effect on PCMI cladding failure and scale data between BWR "cold" conditions and PWR "hot" conditions.

It should be noted that the PWR failure thresholds developed in this report are not only applicable to RIA events starting at HZP conditions, based on the data at essentially HZP, but are also applicable to RIAs starting at an initial power greater than zero with the primary coolant "hot," therefore, the PWR failure thresholds are sometimes referred to as for "hot" initial conditions.

Definitions of energy deposited, peak enthalpy change, and enthalpy change at failure follow.

- The energy deposited is the measured power deposited in the test rodlet.
- The peak radially-averaged-across-the-fuel enthalpy change is the enthalpy increase during the test.
- The enthalpy increase (or change) at time of failure is the enthalpy at the point (time) of failure.

There is disagreement among experts as to the validity of CABRI test rodlet REP-Na1. A Task Force was established by the Technical Advisory Group to the CABRI project[1] to re-examine the test data but the Task Force was unable to reach technical consensus. In a summary of the main conclusions from the test series (NEA 2010), the TAG excluded the controversial REP-Na1 test, but those conclusions were not significantly altered by the omission. The operator of the CABRI facility (IRSN) continues to include the REP-Na1 test in its summary of the REP-Na test series (Papin et al. 2007) and is included in Appendix A of this report. In addition, analyses by others (Alvis et al. 2010, NRC 2004) note the disagreement and excluded this rodlet in their evaluations of PCMI failure threshold. After consideration of this issue, Pacific Northwest National Laboratory (PNNL) has excluded test rodlet CABRI/Rep-Na1 in the development of the PCMI failure criteria.

Earlier RIA testing performed in the PBF and Special Power Excursion Reactor Test (SPERT)-CDC test reactors has been summarized in other reports (NRC 2004, Alvis et al. 2010, NEA 2010). These test results were not used to develop the PCMI failure criteria in this report because most of these tests were performed on fresh or very low burnup rods where PCMI is not considered the failure mechanism. There were two rods tested in SPERT-CDC tests with a burnup of 32 GWd/MTU, but these had abnormal corrosion and hydriding not representative of current fuel at this burnup. There have been reactivity insertion tests on Vodo-Vodyanoy Energetichesky Reaktor (Russian pressurized water reactor, or VVER) fuel rods in the Impulse Graphite Reactor (IGR) test reactor with pulse widths of 750 to 950 ms and the Bystry Impulsny Graphitovy Reaktor (Russian Fast Pulse Graphite Reactor, or BIGR) test reactor with pulse widths of 2.5 to 3 ms. Neither the IGR nor BIGR test data were included in determining the PCMI failure criteria in this report because failures in these tests were not believed to be because of PCMI. The authors admit that significant engineering judgment was also part of the process of deciding which data to include and which data to exclude from this study.

It should further be noted that the rodlets tested in CABRI and NSRR are limited with few replicate data, such that there is still considerable uncertainty to the PCMI failure criteria developed in this report. Resolution of the long-standing issue related to the cold-to-hot and hot–to-cold adjustments of the data is

[1] CABRI Technical Advisory Group. 2007. "Summary and conclusions on what we learned from the REP NA UO_2 test interpretation (REP Na1 excluded)." Minutes of the Fourteenth Meeting of the Technical Advisory Group of the IRSAN-OECD CABRI Water Loop Project; Aix-en-Provence, France.

particularly critical because there are only two pairs of cold-versus-hot data used to estimate this adjustment, e.g., the standard error on the cold/hot difference in the two pairs is ± 14 cal/g (see Section 3.3); although both pairs demonstrate a similar cold-versus-hot difference in failure enthalpy.

Significant experimental uncertainty arises for some data points. The most extreme example of uncertainty for the CABRI tests is for the CABRI/RepNa8 test rodlet that reported enthalpy at failure between 44 to 78 cal/g (± 17 cal/g) based on different indications of time of cladding failure (Papin et al. 2007 and NEA 2010). The uncertainty for the CABRI/RepNa8 single data point is assumed to be ± 17 cal/g. The time of failure was more definitive for the other two CABRI test rodlets that failed (RepNa7 and RepNa10, both at HZP initial temperature of 285°C) and that reduced the uncertainty to ± 10 cal/g.

It is also noted that very recently a paper by Udagawa et al. 2011 has increased and decreased (only test rodlet BZ2 decreased by more than 3 percent) the total peak radial enthalpies for some NSRR PWR test rodlets from those provided in NEA 2010. The increase is not large for most of the failed rodlets, but the two that increased significantly were HBO1 from 73 cal/g (306 J/g) to 124 cal/g (518 J/g) and TK2 from 107 cal/g (448 J/g) to 163 cal/g (683 J/g). This is significant because as will be noted below in our LSQ fit of the CWSRA data, these two data (HBO1 and TK2) resulted in much lower failure enthalpies than the other data. Increasing their failure enthalpies will provide better agreement with the other data and a better LSQ fit (very similar fit but lower uncertainty). The VA3 rodlet also increased to a lesser amount from 108 cal/g (454 J/g) to 123 cal/g (515 J/g). The (BZ2) failed rodlet total deposited enthalpy went down from 154 cal/g (644 J/g) to 130 cal/g (582 J/g). These changes in total deposited enthalpy will most likely change the failure enthalpies for these rods particularly if the change in failure enthalpy is proportional to the change in total enthalpy. A refit of the PWR failure threshold in Section 3.10 has been performed assuming there is a direct proportionality between the change in failure enthalpy and total enthalpy deposited. This increased the PWR failure threshold by approximately 6.4 cal/g at 100 weight parts-per-million (wppm) of excess hydrogen and 6.2 cal/g at 800 wppm.

Two non-failed rodlets, BZ3, and VA4 also increased approximately by 12 percent, and the RH2 non-failed rodlet increased by approximately 19 percent. Neither of these non-failed rodlets changes the failure threshold developed here because the threshold is only based on the failed rodlet data.

2.1 Uncertainty in the Data

The uncertainty in the peak fuel enthalpy change at failure and hydrogen in the cladding have been estimated. The peak fuel enthalpy increase versus time is calculated with a fuel performance code such as FRAPTRAN-1.4 (fuel rod analysis program for transients) (Geelhood et al. 2011) or SCANAIR (Federichi et al. 2000) with total energy deposited as determined during the pulse period along with pulse width (shape) used as input to the codes. The peak enthalpy increase versus time was used along with the time of failure as determined from the microphone signal(s) to determine the peak fuel enthalpy increase at failure. The uncertainty in the total energy deposited is related to uncertainties in measured reactor power and the measurement of the coupling factor between core and test assembly power. The uncertainty in the total energy deposited is approximately 7 percent while the uncertainty in the code calculated energy increase (delta) at failure is approximately 10 percent (includes uncertainty in timing of failure and code calculation) with a minimum total uncertainty of ± 10 cal/g for failure enthalpies below 100 cal/g (Petit et al. 2007). The exception to this uncertainty in enthalpy at failure is for the

CABRI/RepNa8 test rodlet because the point in time for failure was not well identified such that failure occurred somewhere between 44 cal/g to 78 cal/g (note that enthalpy increases with time during these tests). The greater uncertainty in failure for this test rodlet is because the test had several microphone events at different times during the test that suggested cladding cracking started at the time 44 cal/g was deposited, but gas pressure was not lost until 78 cal/g was deposited, as determined by pressure sensors and flow meters.

The uncertainty in the measured hydrogen is difficult because in most cases the measurement is performed from an axial ring cut at an axial position on the father rod near the position in which the test rodlet was cut. The measurement is performed by melting the cladding ring in a vacuum and collecting the gas. It is known that hydrogen can vary considerably both circumferentially and axially because it diffuses to cold regions in the cladding such that it does not always remain where it originated. A full ring of cladding should reduce the circumferential variability. Therefore, there is an uncertainty in the hydrogen measurement because the measurement was not performed at the axial location where failure in the rodlet was experienced. The uncertainty in the measured hydrogen levels is assumed to be 100 wppm for Zr-4 and ZIRLO™ and 40 wppm for M5 and E110. The uncertainty in the measured hydrogen values is based on variations in observed axial averaged hydrogen over 1.0-inch to 0.5-inch increments along a 12.0-inch-to-18.0-inch length of fuel cladding.

A higher uncertainty exists for samples where hydrogen is calculated from measured oxide thickness based on hydrogen pickup fraction for PWRs. For these specimens, hydrogen uncertainty in terms of percent error (not in wppm hydrogen) is based on the measured oxide thicknesses and measured hydrogen data provided in (Geelhood and Beyer 2011). The standard deviation for PWR cladding pickup fraction is calculated to be 23 percent for Zry-4 and ZIRLO™ above approximately 25 μm oxide thickness and 29 percent for M5. Geelhood and Beyer (2011) provided standard deviation in terms of wppm of hydrogen, but more recent PNNL analyses suggest that standard deviation for hydrogen is best represented in terms of percent of measured value.

The uncertainty in predicted hydrogen values for the BWR Zr-2 RXA cladding is assumed to be 60 wppm absolute uncertainty for BWR rods with burnups greater than 49 GWd/MTU (Geelhood and Beyer 2011); all of the BWR failed test rodlets had burnups greater than 60 GWd/MTU. Analysis of the BWR data suggests that standard deviation is best represented in terms of wppm of measured hydrogen. The BWR and PWR hydrogen uncertainties in predicted values were based on a statistical evaluation of the data compiled by Geelhood and Beyer (2011).

3.0 PWR PCMI Threshold

Appendix A provides the hot and cold PWR test data, the measured total hydrogen values are provided when measured, but most values of hydrogen were not measured and are calculated from the measured oxide thicknesses using a pickup fraction that is alloy-dependent. The assumed pickup fraction for each PWR alloy is

- Zry-4 CWSRA: 0.153
- M5™: 0.10
- ZIRLO™: 0.173.

The Zry-4, M5™, and ZIRLO™ pickup fractions are the same as those provided by Geelhood and Beyer (2011). The pickup fraction for ZIRLO™ was increased in FRAPCON from 12.5 to 17.3 percent for this analysis, based on a recent reevaluation of all the pickup fractions in FRAPCON-3.4 (Geelhood et al. 2010) relative to the latest high burnup data (Geelhood and Beyer 2011) including the measured hydrogen for the ZIRLO™ rodlets for these RIA tests.

Sections 3.1 through 3.9 discuss the impact of the following items on the PCMI failure threshold for a PWR RIA "hot" event:

- the range of peak fuel enthalpy change and hydrogen levels in the cladding
- the effects of hydrogen/corrosion
- hot versus cold
- cladding type
- burnup
- fuel type (UO_2 and MOX)
- pulse width
- fuel-clad gap size
- oxide spallation.

Sections 3.10 and 3.11 describe the PCMI failure thresholds for a PWR RIA hot event from a best-estimate LSQ fit of the CABRI and NSRR test data for CWSRA and RXA cladding, respectively. A comparison of the CWSRA failure threshold from the LSQ fit is made to the PWR threshold in Appendix B of the Standard Review Plan (SRP) 4.2 (NRC 2007). Section 3.12 will describe the applicability of these failure thresholds to pRXA zirconium alloy cladding. Additionally, limitations for these thresholds will be stated in Section 3.14

3.1 Range of Fuel Enthalpy and Hydrogen Levels Tested for PWR Rodlets

The majority of the PWR RIA tests were performed with UO_2 fuel and Zry-4 cladding. The range of these data in terms of peak fuel enthalpy change and excess hydrogen is demonstrated in Figure 3.1. Note

that in Figure 3.1 both dependent (enthalpy change) and some of the independent (excess hydrogen) variables are calculated rather than measured values. The range of all the PWR data (includes UO_2 and MOX fuel with Zr-4 ZIRLO™ or M5™ cladding) is provided in Figure 3.2, which demonstrates that maximum enthalpy tested was 180 cal/g at low hydrogen levels (< 30 wppm), and maximum excess hydrogen was 800 wppm at 80 cal/g peak fuel enthalpy for all test rodlets tested in NSRR and CABRI. If only the UO_2 data are considered, the peak fuel enthalpy change is limited to 105 cal/g above 190 wppm excess hydrogen (Figure 3.1), however, adding the MOX and ZIRLO™ test rodlets increases the range of maximum peak enthalpy above 190 wppm excess hydrogen by a considerable amount, to 165 cal/g peak fuel enthalpy change (Figure 3.2).

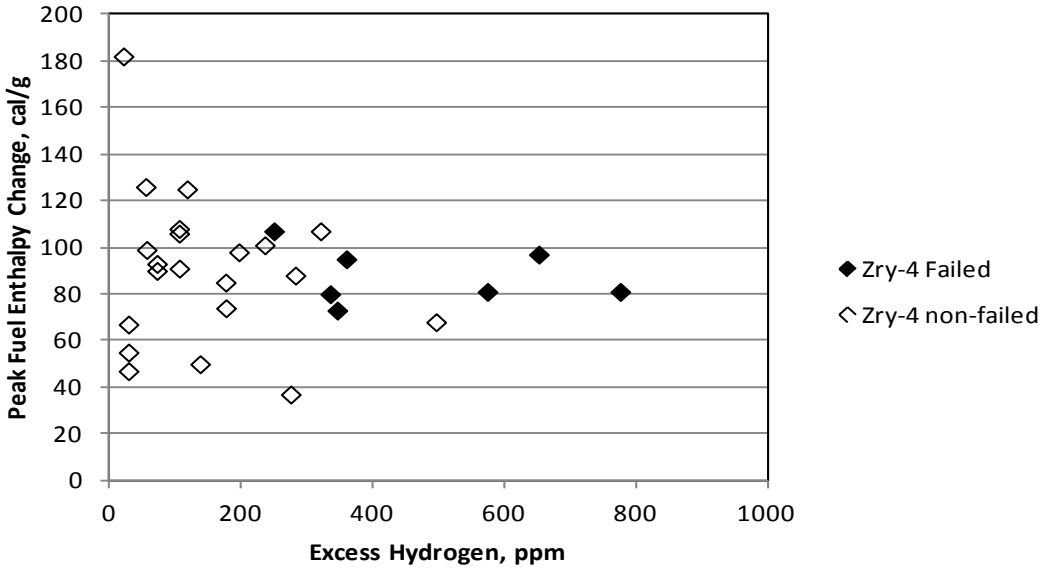

Figure 3.1. Range of Peak Total Enthalpy Change Deposited in the Fuel versus Excess Hydrogen (measured or calculated if not measured) for UO_2 PWR Test Rods with Zry-4 Cladding

These tests were conducted with pulse widths between 4.4 and 75 ms; see Section 3.7 for discussion of the impact of pulse width on failure threshold. Note that the four M5™ test rods in Figure 3.2 never exceeded 110 cal/gm peak fuel enthalpy change, nor exceeded 100 wppm hydrogen, none of these four rods failed. The lack of failure may be because of the low enthalpy and low hydrogen level for these tests. The reason that the M5™ tests rods did not exceed 110 cal/g peak fuel enthalpy change is because all of these rods were at high burnup levels (≥ 60 GWd/MTU) such that their reactivity was limited.

All test rods in Figure 3.3 are plotted in terms of the peak enthalpy change at failure or total peak fuel enthalpy change if not failed versus excess hydrogen. For example, Figure 3.3 is different than Figure 3.2 because the y-axis is peak fuel enthalpy change at failure for failed rods, not the total enthalpy change depicted as in Figure 3.2. All rods have UO_2 fuel in Figure 3.3 unless identified as MOX. The CABRI/RepNa8 test rodlet time of failure was not well identified such that failure occurred somewhere between 44 cal/g to 78 cal/g that is illustrated in Figure 3.3 as error bars. The uncertainty in failure is because this test had several microphone events that suggested the cladding cracking started at 44 cal/g but gas pressure was not lost until 78 cal/g. Subsequent plots will represent this datum as the mean of 44 and 78, or 61 cal/g.

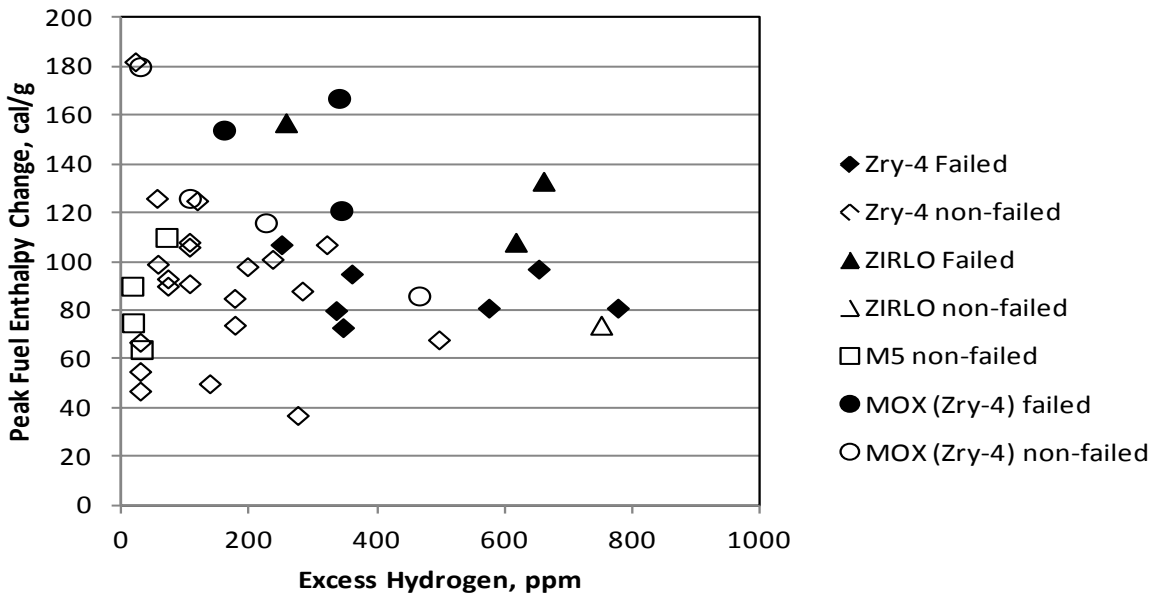

Figure 3.2. Range of Peak Total Enthalpy Change Deposited in Fuel versus Excess Hydrogen for UO_2 and MOX Test Rods with Zry-4, ZIRLO™ or M5™ Cladding

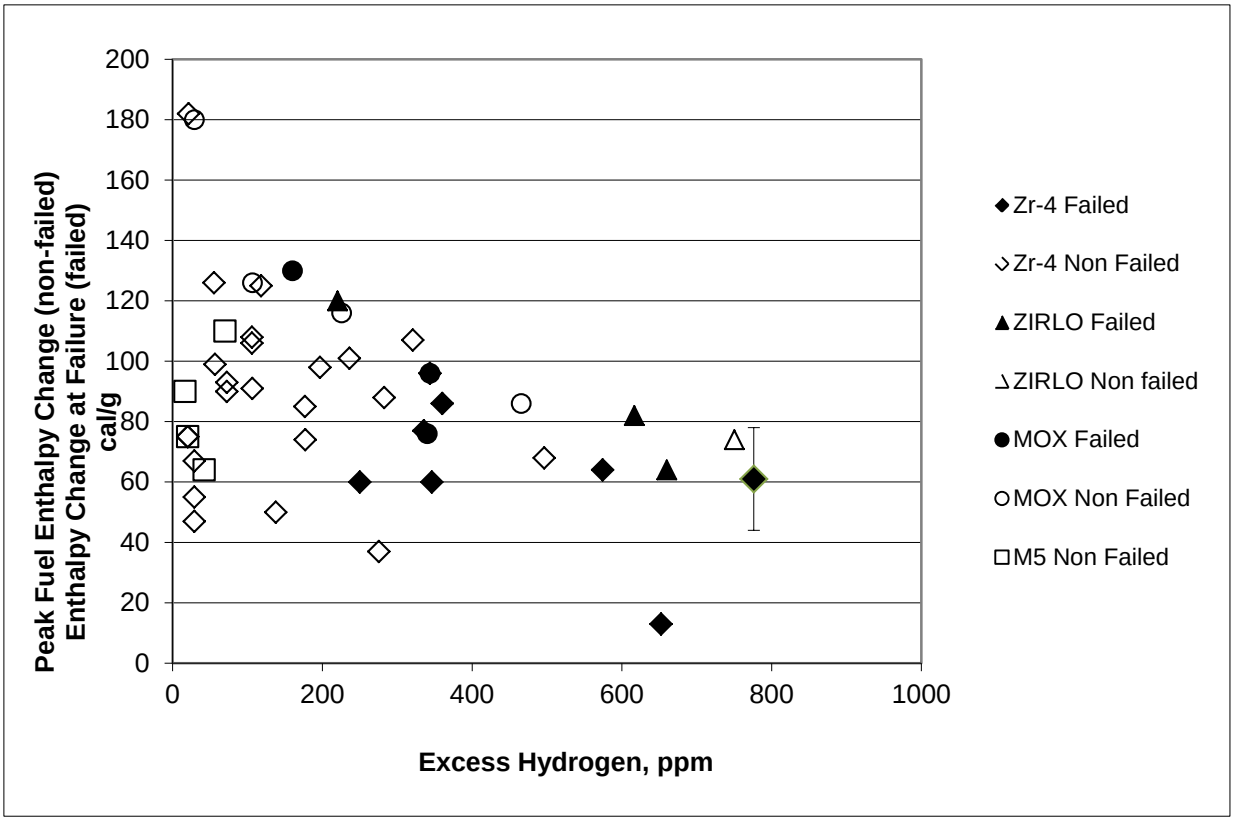

Figure 3.3. Peak Fuel Enthalpy Change at Failure (for failed rods only) versus Excess Hydrogen for all PWR Test Rod Results with No Adjustments to Data (open points are non-failed and closed points are failed test rods)

3.2 Hydrogen/Corrosion Effects

The PWR RIA failure threshold is shown to have a strong correlation of decreasing fuel enthalpy change with increasing excess hydrogen in the cladding, as illustrated in Figure 3.4 for UO_2 test rodlets with Zry-4 cladding, e.g., the failure threshold is above 180 cal/g at low hydrogen (< 60 wppm) based on one data point and decreases to between 60 and 90 cal/g by 350 wppm excess hydrogen. The non-failed rods are the open diamonds and failed rods are closed diamonds. The hydrogen level for PWRs is a function of cladding corrosion because the oxidation reaction creates two hydrogen atoms according to the reaction:

$$Zr + 2H_2O \rightarrow ZrO_2 + 2H_2 \quad (1)$$

For the PWR cladding, Zry-4, ZIRLO™, and M5™, it has been found that the hydrogen content in the cladding can be accurately modeled by using a constant pickup fraction. The pickup fraction for each cladding type is discussed above in Section 3.0.

Both oxidation and hydrogen levels generally increase with increasing burnup. Excess hydrogen is that hydrogen above the solubility limit that precipitates out as zirconium hydride. The following equation (Kearns 1967) can be used to determine the hydrogen that is in solution

$$H_{sol} = 1.2 \times 10^5 \exp\left(\frac{-8550}{1.985887 \cdot T}\right) \quad (2)$$

In this equation, T is in K and H_{sol} is in wppm. The hydrogen solubility at 280°C is approximately 70 wppm. All hydrogen values in figures are measured (if range of measured values is given, then an average value is used for the LSQ fits) or calculated from oxide thickness if not measured using the pickup fractions discussed above.

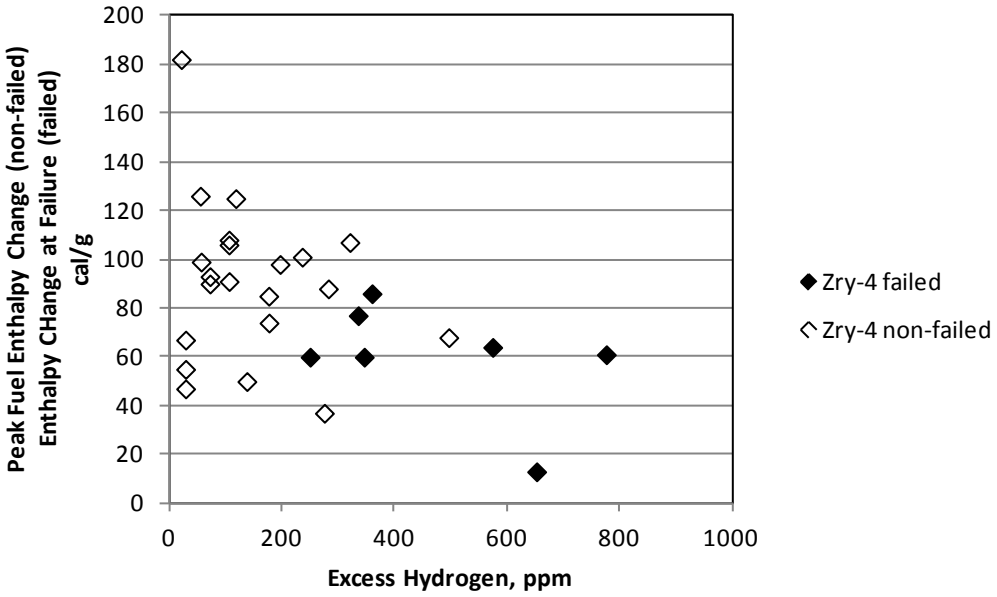

Figure 3.4. Peak Fuel Enthalpy Change at Failure (for failed rods) versus Excess Hydrogen (measured or calculated if not measured) for Test Rods with UO_2 and Zry-4 Cladding (open symbols are non-failed and closed symbols are failed test rods)

3.3 Hot Versus Cold Test Effects

There has been a long-standing question on whether initial cladding temperature has a significant impact on the cladding failure threshold and if so, what is the quantitative effect between HZP and CZP? It is important to understand temperature effects in order to scale the room temperature NSRR test results to PWR "hot" operating conditions and the CABRI test results to BWR "cold" startup conditions (CZP). The scaling of temperature effects is necessary because of the limited amount of "hot" and "cold" test data applicable to PWR "hot" and BWR "cold" (CZP) conditions.

Examination of the failed test rods at both "hot" and "cold" conditions and similar hydrogen levels in Figure 3.3 identifies two hot and cold rodlet pairs at similar hydrogen levels that failed and can be used to determine the existence and magnitude of a difference in hot-versus-cold impact on failure threshold.

These pairs are shown in Table 3.1. One pair is two MOX rods with Zry-4 cladding, CABRI/RepNa7 (hot) and NSRR/BZ1 (cold) both at approximately 340 wppm excess hydrogen that failed at 96 cal/g and 76 cal/g, respectively, with a differential of 20 cal/g in failure threshold. The second pair is two UO_2 rods with ZIRLO™ cladding, NSRR/VA-3 (hot) and NSRR/VA-1 (cold) were at 617 wppm and 660 wppm excess hydrogen, respectively, that failed at 82 cal/g and 64 cal/g, respectively, with a 18 cal/g differential in failure threshold. Both NSRR/VA-1 and NSRR/VA-3 had a similar pulse width of 4.4 ms while CABRI/RepNa7 and NSRR/BZ1 had 4.4 ms and 40 ms pulse widths, respectively. The effect of pulse width will be examined in Section 3.7 with a conclusion that the failed test data do not demonstrate a pulse-width effect. These two data pairs give similar values of 18 cal/g and 20 cal/g for hot versus cold effects. FRAPTRAN 1.4 calculates a difference between hot and cold of approximately 9 cal/g just from the hydrogen solubility differences between 20°C and 280°C.

Table 3.1. Hot and Cold Rodlet Pairs at Similar Hydrogen Levels

Rod	Fuel	Cladding	Excess Hydrogen	Coolant	Pulse Width	Enthalpy Increase at Failure	Difference
RepNa7	MOX	Zry-4	340 wppm	Hot	40 ms	96 cal/g	20 cal/g
BZ1	MOX	Zry-4	340 wppm	Cold	4.4 ms	76 cal/g	
VA3	UO_2	ZIRLO™	617 wppm	Hot	4.4 ms	82 cal/g	18 cal/g
VA1	UO_2	ZIRLO™	660 wppm	Cold	4.4 ms	64 cal/g	

MOX = mixed uranium and plutonium dioxide

Based on the comparisons in Table 3.1, it is concluded that the data may be adjusted by 18 cal/g to account for the differences between hot conditions and cold conditions. This same adjustment is applied to RXA cladding. The cold NSRR failed test data have been adjusted upwards by 18 cal/g in Figure 3.5 (shown as large symbols), in agreement with the two pairs of NSRR and CABRI data tested at hot and cold conditions. The cold NSRR failed tests without an adjustment to conditions are also shown in Figure 3.5 as small symbols. A comparison of these points in Figure 3.5 demonstrates that the cold-to-hot adjustment of the failed NSRR cold tests provides less scatter between the hot and cold tests and, therefore, appears to be justified. The two tests in Figure 3.5 that deviate from the others are NSRR/TK2 (250 wppm/ 78 cal/g) and CABRI/Na1 (652 wppm/13 cal/g). CABRI/Na1 has been eliminated by PNNL in the development of the PCMI failure threshold in this report. It will also be eliminated in the curve fitting to be discussed in Section 3.10 that proposes a PWR "hot" failure threshold for CWSRA. The NSRR/TK2 test has been retained for the LSQ fit in Section 3.10.

The report by Alvis et al. 2010 has also developed a cold-to-hot adjustment for this same PWR data but the adjustment has a strong dependence on hydrogen level based on those investigators' own fuel performance code calculations. This report does not quantitatively define their cold-to-hot adjustment versus hydrogen level, but does provide some fuel performance code calculated results in terms of peak delta failure enthalpy at six different hydrogen levels in Figures 4-13 and 4-14 of the Alvis et al. (2010) report. Scaling their hot (280°C) versus cold (20°C) calculations of delta enthalpy from Figures 4-13 and 4-14, the adjustment appears to be approximately 36 to 44 cal/g at 360 to 475 wppm of hydrogen and 25 to 28 cal/g at 650 to 750 wppm of hydrogen. However, their adjustment is significantly higher than the two hot (280°C initial cladding temperature) versus cold (20°C initial cladding temperature) data pairs in Table 3.1 at similar hydrogen levels, where the hot-versus-cold difference is only 20 cal/g at 340 wppm hydrogen and 18 cal/g at 617 to 660 wppm hydrogen.

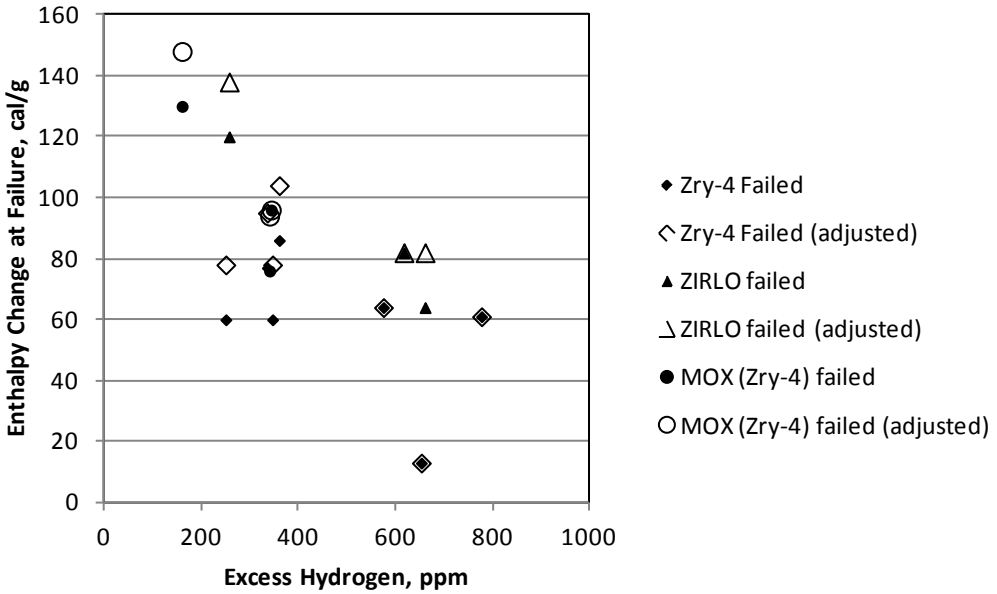

Figure 3.5. Peak Fuel Enthalpy Change versus Excess Hydrogen for all PWR Failed with Cold Rods Adjusted Upward by 18 cal/g to Account for Hot Zero Power Conditions for PWRs and with Cold Tests Not Adjusted. (Points labeled "adjusted" include cold rods that were adjusted and hot rods that were not adjusted.)

The report by Alvis et al. 2010 also has a temperature adjustment for the failure threshold for a BWR CZP RIA. This report suggests that the ductile brittle transition temperature (DBTT) for Zr-2 RXA cladding is 80°C to 85°C, based on data that were not presented or referenced. The report further proposes that a BWR RIA event that initiates near room temperature (CZP) the cladding will be near 85°C or greater by the time PCMI is experienced. As a result the report increases BWR CZP failure threshold for Zr-2 RXA cladding from the NSRR tests by approximately 22 cal/g at 150 to 200 ppm and by approximately 15 cal/g at 300 ppm, assuming the DBTT is 85°C.

Examination of two NSRR test rods with irradiated Zr-2 RXA cladding suggests that the DBTT is > 95°C and open literature testing of DBTT of irradiated Zr-2 RXA cladding suggests that it is > 200°C. The two NSRR BWR test rods were FK10 and FK12 (Zr-2 RXA) tested with initial coolant temperatures of 80°C and 85°C, respectively (NEA 2010). No difference in failure mode was observed in these Zr-2 RXA rods from those tested at 20°C (NEA 2010). The cladding temperatures typically increase only by a small amount for NSRR tests at the failure enthalpy levels for these rods but it is typically greater than 10°C. Therefore, the cladding temperatures for FK12 were greater than 95°C at failure suggesting that the ductile-to-brittle transition for irradiated Zr-2 RXA is above this temperature from these RIA tests.

A paper by Kubo et al. (2010) has reported a DBTT for irradiated Zr-2 RXA between 250°C and 300°C for plane strain, applicable to PCMI. Based on the FK10 and FK12 NSRR BWR tests and Kubo et al. (2010), it is concluded that a temperature adjustment for a BWR CZP RIA is not justified.

The uncertainty in the cold-to-hot adjustment is judged to be significant because it is based on only two hot/cold data pairs and as noted in Section 2.1, there may be an adjustment in failure enthalpy for the VA3 rodlet. The 18 cal/g adjustment has been estimated assuming that both the hot and cold

measurements individually have a ± 10 cal/g uncertainty as discussed in Section 2.1. If it is assumed that these uncertainties are normal and not biased (assumption may not be true because a bias may exist) then the hot and cold measurement uncertainties can be statistically combined for the data pairs to give an uncertainty of $(10^2 + 10^2)^{0.5} \approx 14$. Therefore, the hot/cold adjustment of 18 cal/g is estimated to have a standard error of ± 14 cal/g if measurement uncertainties are normal and not biased.

Examination of the two hot and cold MOX rods at 340 wppm and the two cold UO_2 failed rods at a similar hydrogen level in Figure 3.5 also demonstrates that the MOX tests are within scatter of the UO_2 tests; this will be discussed further in Section 3.6.

3.4 Cladding Type (Zry-4 CWSRA, ZIRLO™ CWSRA, and M5™ RXA) Effects

Examination of the failed test rodlets in Figure 3.3 with Zry-4 CWSRA (seven rods) and ZIRLO™ (three rods) cladding suggest that there is no discernible difference in the failure threshold for these two cladding types at similar excess hydrogen levels. However, it should be understood that the analysis of cladding type conducted in this study has been heavily informed by a comparison of Zry-4 CWSRA and ZIRLO™ CWSRA mechanical test data provided by Geelhood et al. (2008) that demonstrated similar properties for these two cladding materials. Westinghouse recently introduced a low-tin ZIRLO™ (Optimized ZIRLO™) that does not have a CWSRA heat treatment but is instead pRXA. No mechanical property test data are available nor are there data on the hydride orientation of Optimized ZIRLO™ found in the open literature. In the absence of data, it is recommended that Westinghouse be required to use the M5™ correlation for Optimized ZIRLO™ (pRXA) unless they can show data from irradiated Optimized ZIRLO™ that demonstrate that the hydrogen morphology in and uniform elongation of Optimized ZIRLO™ are the same as that of ZIRLO.™

None of the four M5™ test rods failed at peak fuel enthalpies up to 110 cal/g (excess hydrogen levels $\leq$ 70 wppm), which is consistent with the Zry-4 CWSRA test rods with UO_2 or MOX fuel at similar hydrogen levels where no failure was observed up to 180 cal/gm. Therefore, it is not possible to compare failure threshold for M5™ RXA compared to those for Zry-4 and ZIRLO™ because no failures were experienced for M5™ at the low enthalpy and hydrogen levels tested. However, Sections 3.10, 3.11, 4.3, and 4.4 will demonstrate that the Zry-2 RXA cladding has a lower failure threshold than the Zry-4 CWSRA cladding. The reason for this difference is believed to be because of differences in hydride orientation for RXA versus CWSRA cladding types. The M5™ cladding is RXA and will have a similar hydride distribution as for Zry-2 RXA with the exception that M5™ cladding will not have hydrides collected at the cladding inner diameter (ID) as is the case for BWR Zr-2 RXA with a liner at high burnups. The presence of hydrides on the ID of RXA cladding could result in some embrittlement at the ID for the BWR test rodlets at high burnup. Therefore, applying the BWR Zr-2 RXA test rodlets to derive an M5™ RIA failure threshold would result in a more conservative threshold for M5™ cladding; however, because of the lack of test rodlets with M5™ cladding that have failed, the BWR Zr-2 RXA data will be used. The M5™ data will be placed with the Zr-2 RXA data in this evaluation with appropriate adjustments for “hot” or “cold” conditions.

The thresholds developed in this report may not apply to a new cladding type with different hydride distribution or orientation than those tested in this report. For example, if a newly developed RXA cladding no longer has hydrides randomly orientated, this may increase the failure threshold compared to

the existing RXA cladding types in this report. This cladding would have to be tested at service conditions similar to those for a RIA event to determine if there is justification for a change in the failure threshold.

3.5 Burnup Effect

In order to examine if there is a dependency of enthalpy increase at failure with burnup Section 3.10 has examined the residuals from the LSQ fit to hydrogen by plotting the residuals versus burnup to determine if the residuals demonstrate a trend (dependence) with burnup. The residuals plotted in Section 3.10 demonstrate that there may be a very weak dependence with burnup that shows a negative slope and a poor R^2 value equal to 0.21. This slope of -0.724 will result in a higher failure threshold for higher burnup fuel if the hydrogen level remains constant. The negative slope with burnup is difficult to explain unless there is increased compliance (softening) of the fuel with burnup that has not been demonstrated experimentally. This dependence with burnup may not be real because of the poor R^2 value, the small amount of data, and the natural uncertainty (scatter in the data), and it is primarily because of one datum. The weak burnup dependence observed is primarily because of the NSRR/TK2 datum that provides a significantly lower threshold than the other data near this hydrogen level. When this one-test datum is removed, the negative slope is significantly reduced by nearly a factor of 2 and R^2 is reduced to 0.13. Therefore, a burnup dependence is not included in the PWR PCMI failure threshold for "hot" initial conditions.

3.6 MOX Effects

One report (Alvis et al. 2010) concluded that MOX fuel rods will have a lower PCMI threshold from gaseous swelling in MOX because it introduces higher cladding strains than UO_2 rods for a given enthalpy change. The higher cladding strains have been observed in the RIA tests of non-failed MOX rods. However, examination of the UO_2 and MOX failed test rodlets discussed below have not suggested there is a significant difference in PCMI failure threshold for the RIA tests.

All of the UO_2 and MOX tests failed and non-failed are plotted in Figure 3.6 with the NSRR cold tests adjusted upward by 18 cal/g, as discussed in Section 3.3. Examination of Figure 3.6 demonstrates that the non-failed MOX tests lie within the non-failed UO_2 tests, and more importantly, the failed MOX tests lie within the UO_2 failed tests. This is also demonstrated in Figure 3.5. For example, the two MOX failed tests at 94 cal/g (NSRR/BZ1) and 96 cal/g (CABRI/Na7) with both at approximately 340 wppm excess hydrogen are within the scatter of the three UO_2 tests at 335 wppm/95 cal/g (NSRR/HBO5), 346 wppm/78 cal/g (NSRR/HBO1) and 360 wppm/104 cal/g (NSRR/TK7). The similarity between the failed MOX and UO_2 tests will be discussed again in the development of a "hot" failure threshold for CWSRA cladding. For example, see Section 3.10 where it is noted that there is very little difference in the failure threshold correlation when the MOX tests are included or not included in the LSQ fit but including the MOX tests increases the quality, i.e., decreases the standard deviation, of the LSQ fit. There is no evidence from the RIA failure test data from CABRI and NSRR that the MOX failure threshold is lower than for UO_2.

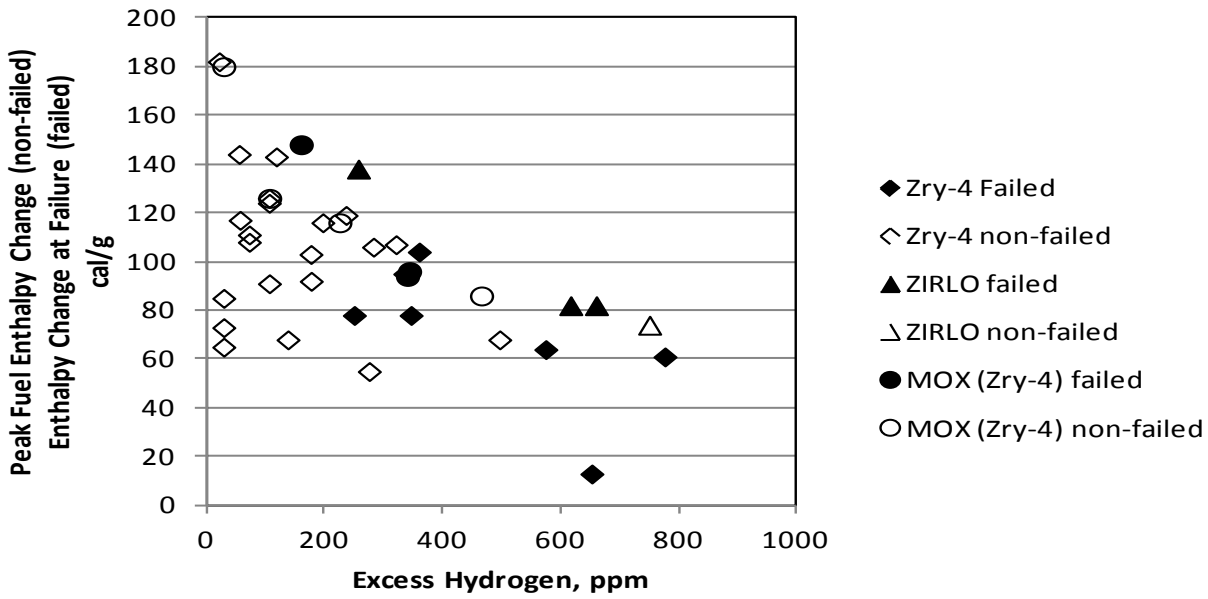

Figure 3.6. Peak Fuel Enthalpy Change versus Excess Hydrogen for All PWR Failed and Non-failed Rodlets with Cold Tests Adjusted Up by 18 cal/g for Hot Conditions

The higher cladding strains observed in non-failed MOX test rodlets are most likely experienced during cladding heatup that happened after the peak PCMI cladding strains were experienced. Therefore, either the gaseous swelling is not significant early in the RIA test, or the cladding has sufficient strength prior to heatup to prevent the gaseous swelling from introducing significant cladding strain.

Vitanza and Conde-Lopez (2004) also found no significant differences in PCMI failure behavior between UO_2 and MOX at fuel enthalpy less than 120 cal/g. Similarly the NEA (2010) report on RIA concluded (in Sections 6.1.2 and 6.2.2) that MOX gaseous swelling does not have a significant effect on failure during the early heat-up phase where PCMI is the dominant failure mechanism. The authors also came to a similar conclusion from this report's analysis, that gaseous swelling has an impact on cladding strain later in the RIA event, during cladding heatup when cladding ballooning and rupture is the failure mechanism.

3.7 Pulse Width Effects

The CABRI tests were the only tests that varied pulse width between 8.8 and 76 ms that bound the pulse width range of U.S. LWR RIA events. All of the NSRR tests had narrow pulse widths close to 4.4 ms. The IGR varied pulse widths between 750 and 950 ms but these are significantly different than prototypical of a RIA event in U.S. LWRs between pulse widths of 10 and 45 ms. Because of the limited failure data (3 CABRI tests and 10 NSRR tests) it is difficult to find similar hydrogen levels with differing pulse widths. However, two failed tests CABRI/Na7 (40 ms) and NSRR/TK7 (4.4 ms) had similar excess hydrogen of 393 wppm and 360 wppm, respectively, and similar failure thresholds of 96 cal/g and 104 cal/g (adjusted cold-to-hot for NSRR/TK7), respectively. The CABRI/Na7 with a pulse width of 40 ms had the lower failure threshold than NSRR/TK7 with a width of 4.4 ms, which is the opposite of what would be expected from code analyses discussed below. Two other failed tests that are not as close in hydrogen level are the CABRI/Na8 (75 ms) and CABRI/Na10 (31 ms) with excess

hydrogen levels of 776 wppm and 574 wppm, and similar failure thresholds of 61 cal/g and 64 cal/g, respectively.

Section 3.10 provides a LSQ regression fit to the CWSRA failure data as a function of excess hydrogen level. The residuals (model predicted minus measured) of this fit plotted versus pulse width demonstrate that there is no obvious bias with pulse width between 4.4 and 76 ms (pulse width range of NSRR and CABRI data) and that excess hydrogen accounts for the variability of the various test data at different pulse widths.

Analyses with fuel performance codes predict that average cladding temperatures will increase with pulse widths greater than 20 ms and the higher cladding temperatures should increase the failure threshold. For example, FRAPTRAN calculations have been performed assuming a standard 17x17 PWR rod with Zry-4 CWSRA cladding. At 40 GWd/MTU the predicted failure enthalpy was 100 cal/g with a 5 ms pulse, and 145 cal/g with a 30 ms pulse (45 cal/g increase from 5 to 30 ms). At 60 GWd/MTU the predicted failure enthalpy was 81 cal/g with a 5 ms pulse and 105 cal/g with a 30 ms pulse (a 24 cal/g increase from 5 to 30 ms). Examination of the data with different pulse widths does not show this dependence. There may be a small dependence because of pulse width, but it cannot be discerned from the uncertainty in the data. This current evaluation of PWR failure threshold concludes that the empirical correlation should be used with no adjustment for pulse width.

One possible reason for this difference between the data and analyses may be in the difference in how failure is initiated in a RIA event with high-hydride levels and how the FRAPTRAN code determines cladding properties to determine failure based on uniform elongation strain measurements. The FRAPTRAN code determines the cladding properties including uniform plastic strain at failure based on averaging the cladding temperatures of all the radial cladding nodes. The code does not consider different cladding deformation limits (plastic versus brittle) for different radial cladding nodes. This approach may not be valid, based on examination of micrographs of failed high burnup cladding that demonstrate an initial crack develops in the brittle hydride rim at the outer diameter and a portion of the inner layer, then ductile failure through the remaining inner cladding (Suzuki et al. 2009). Therefore, from this analysis it is concluded that either the ductility (fracture toughness) of the hydride rim is not sensitive to temperature, or the rim temperature does not increase sufficiently before the crack initiates in a 75 ms pulse to increase the ductility (fracture toughness) of the hydride rim. The difficulty in performing the analysis based on fracture toughness of the rim is that fracture toughness is not well known as a function of temperature for the rim structure nor is it known at the various levels of hydride in the inner portion of the irradiated cladding. Recent modeling has been performed using assumed fracture toughness values for the rim and inner portion of the cladding that have had some success in predicting fracture at cold and hot test conditions (Udagawa et al. 2011).

3.8 Initial As-Fabricated Fuel-Clad Gap to Diameter Effects

The effect of gap size or g/d (fuel clad gap-to-diameter) on the pellet-clad-mechanical interaction failure threshold during a RIA cannot be evaluated by examination of the RIA test data because all of the rods have burnups greater than 33 GWd/MTU above which hard contact has been established between the fuel and cladding during in-reactor operation at normal commercial rod powers. Therefore, the effect of initial fabricated gap size has been examined using the FRAPCON-3.4 (Geelhood et al. 2010) and FRAPTRAN-1.4 (Geelhood et al. 2011) fuel performance codes. The g/d ratio is believed to have an

impact on PCMI failure threshold because this ratio determines how quickly the gap is closed, resulting in hard fuel-clad contact during fuel rod operation. The PCMI failure threshold will decrease as the gap is reduced until hard contact closure at some point in time/burnup. Two PWR fuel designs have been examined, a Westinghouse 17x17 fuel design with an initial diameter gap size of 7 mils (0.007 inches) and g/d = 1.944×10^{-2}; and a Combustion Engineering (now Westinghouse) 14x14 fuel design with a diametral gap size of 6.5 mil (0.0065 inches) and g/d = 1.477×10^{-2}. These two PWR designs have the largest variation in g/d of those currently under production. The smaller the g/d, the sooner hard gap closure will be experienced for a given rod power history.

The PCMI failure threshold decreases with increasing excess hydrogen (corrosion level), but the hydrogen level versus time/burnup is also dependent on cladding alloy. In order to investigate only the impact of g/d, both designs were assumed to have Zircaloy-4 cladding with a maximum corrosion level of 100 microns (peak oxide) at 60 GWd/MTU rod average burnup, end-of-life. In order to accomplish the desired corrosion level of 100 microns it was necessary to introduce a constant rate of crud deposit with time in the FRAPCON-3.4 code such that at end-of-life for the 17x17 fuel the crud deposit was 0.445 mils thick and 2.44 mils for the 14x14 fuel as calculated with the FRAPCON-3.4 code.

The results of the FRAPCON-3.4 code were used to initialize the FRAPTRAN-1.4 code. Several runs with the FRAPTRAN-1.4 code were necessary for each point in time/burnup to determine the as calculated PCMI failure threshold. The FRAPTRAN code would not calculate PCMI failure for the 17x17 and 14x14 designs, making it impossible to determine a PCMI failure threshold. No failure was predicted by the code because of excessive calculated average cladding temperatures that significantly increased cladding ductility. As a result, a version of FRAPTRAN was created to only use the cladding outside (waterside) temperature to determine cladding mechanical properties. This assumption appears to be supported by examination of micrographs of failed high burnup cladding that have demonstrated that an initial crack develops in the hydride rim of the outer diameter and propagates through the more ductile inner cladding (Suzuki et al. 2009), therefore, the rim and corresponding temperature dictate the cladding response to PCMI.

The current PCMI failure threshold in the Appendix B of SRP 4.2 (NRC 2007) for RIA is a function of oxide-to-cladding thickness ratio; this ratio has been converted to excess hydrogen level for the SRP PCMI threshold as shown in Figure 3.7. The conversion from oxide-to-cladding thickness to excess hydrogen was performed by assuming a 17x17 design with Zry-4 cladding, a 0.594-mm wall thickness, an outer diameter of 9.5 mm and a hydrogen pickup fraction of 0.153 (from Geelhood and Beyer 2011).

The SRP 4.2 PCMI threshold assumes that the failure threshold remains constant at 150 cal/g up to 200 wppm hydrogen and decreases above this excess hydrogen level. Above 150 cal/g it is assumed that failure will be because of ballooning and rupture. The FRAPCON/FRAPTRAN analysis results demonstrated that the gap closed for both the 17x17 and 14x14 designs near or prior to achieving a PCMI failure threshold below150 cal/g. Hard contact gap closure is defined as that point where there is a positive interface pressure between the fuel and cladding as shown in Figures 3.8 and 3.9 versus time in days for the Westinghouse 17x7 and CE 14x14 designs, respectively. Note that when a positive interface pressure is experienced, a positive hoop stress will be introduced in the cladding, this is achieved at approximately 290 days for the 17x17 design (Figure 3.9) for the middle 4 axial nodes (center 4 feet of active fuel) and 170 to 324 days (depends on axial node) for the 14x14 design for the center 8 feet of active fuel (Figure 3.10).

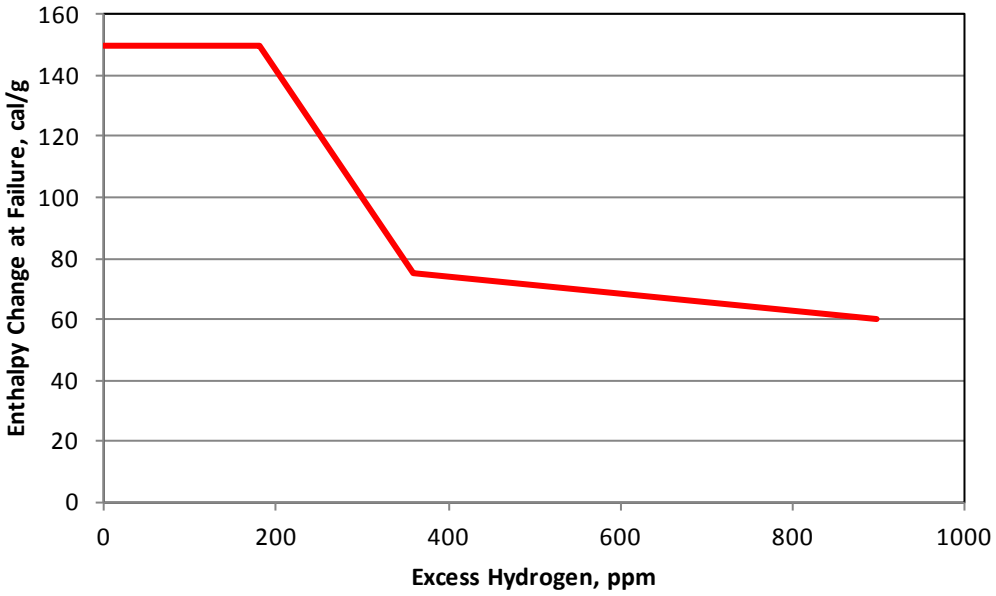

Figure 3.7. Appendix B of SRP 4.2 (NRC 2007) Failure Threshold for PWR RIA Event with Zry-4 CWSRA Cladding in Terms of Excess Hydrogen (the failure threshold in SRP 4.2 is a function of oxide thickness/cladding diameter, this has been converted to excess hydrogen)

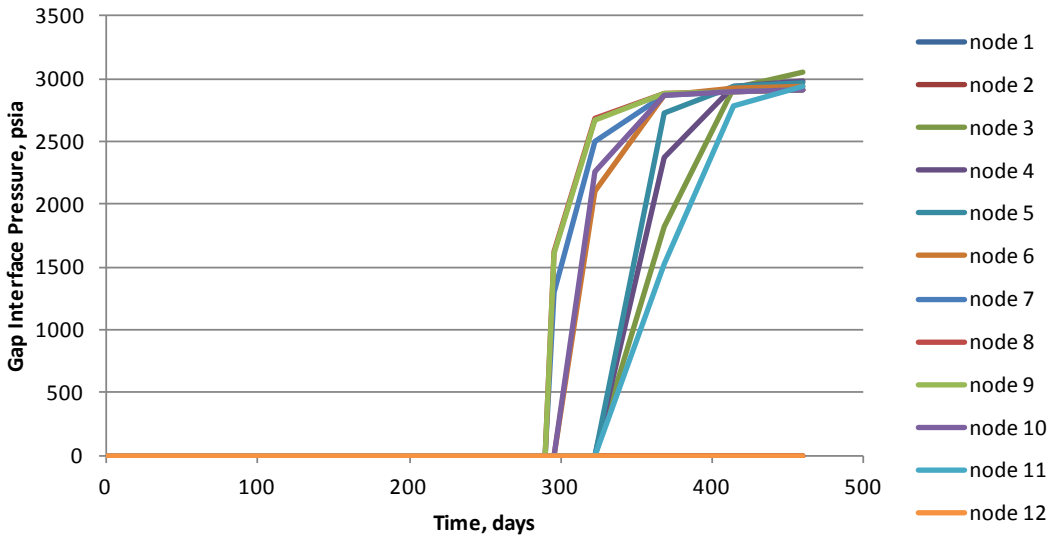

Figure 3.8. Westinghouse 17x17 Hard Gap Closure (positive fuel-clad interface pressure) versus Time (full power days)

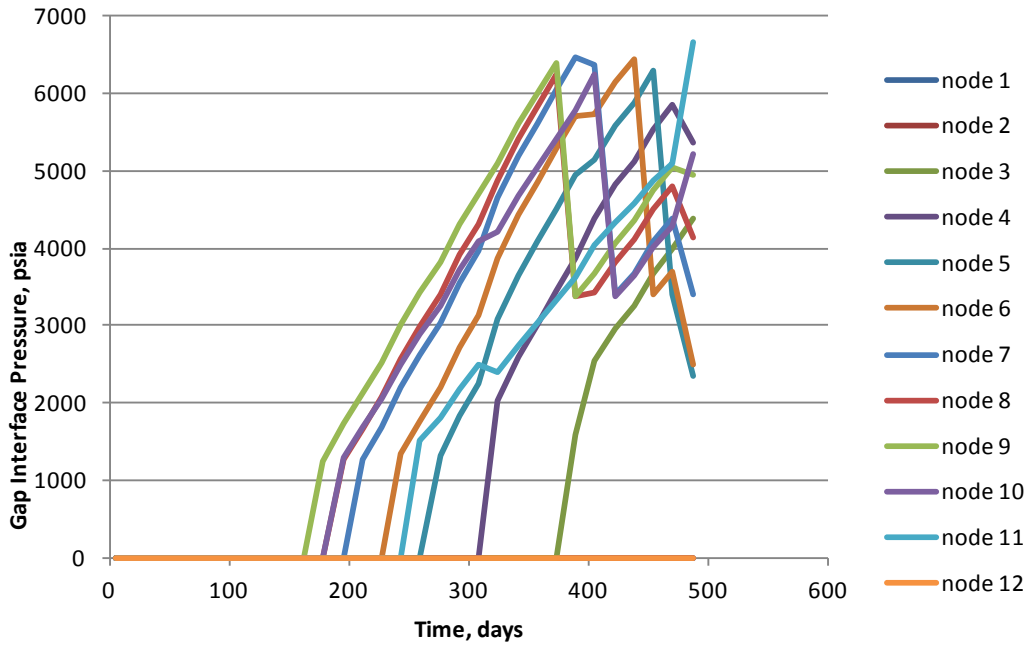

Figure 3.9. CE 14x14 Hard Gap Closure (positive fuel-clad interface pressure) versus time (full power days)

The PCMI failure threshold (as calculated by FRAPCON4.3/FRAPTRAN-1.4) for the Westinghouse 17x17 design versus time and rod average burnup is shown in Figure 3.10. The PCMI failure threshold for the Combustion Engineering 14x14 design versus time and rod average burnup is shown in Figure 3.11. The Westinghouse 17x17 failure threshold drops below 150 cal/g above 18 GWd/MTU (280 days) while the gap (positive interface pressure) at a rod average burnup of 18.4 to 19.2 GWd/MTU (290 to 295 full power days in Figure 3.8) such that gap closure and the 150 cal/g threshold occur at approximately the same point in time for the center 4 feet of active fuel. Within 325 days the center 8 feet of active 17x17 fuel length hard gap closure occurs, i.e., there is a positive interface pressure, such that only a very small gap exists between 280 and 325 full power days. This means that for the 17x17 design, the initial gap size will have no impact on the PCMI failure threshold in Figure 3.8 for the center 4 feet of active fuel, and because the gap is nearly closed for an additional 4 feet of active fuel, the gap will have a small effect on the PCMI failure threshold for this axial region. The Combustion Engineering 14x14 failure threshold dropped below 150 cal/g above approximately 14.5 GWd/MTU (approximately 315 full power days in Figure 3.11) while the gap closed very early for the 14x14 design at a rod average burnup of 8 to 14.5 GWd/MTU (170 to 315 full power days in Figure 3.9) in the center 8 feet of active fuel because of the smaller g/d. The gap closes earlier in the center axial nodes than when the14x14 failure threshold of 150 cal/g is achieved, i.e., approximately 10 GWd/MTU mean burnup for gap closure versus 14.5 GWd/MTU for PCMI failure. Therefore, both designs will most likely fail by ballooning and rupture and not fail by PCMI when the fuel-gap is open during at power operation as calculated with FRAPCON-3.4/FRAPTRAN-1.4 codes. Therefore, the initial as-fabricated g/d either has no effect or has a small effect on the PCMI failure threshold for the center 8 feet of the active fuel.

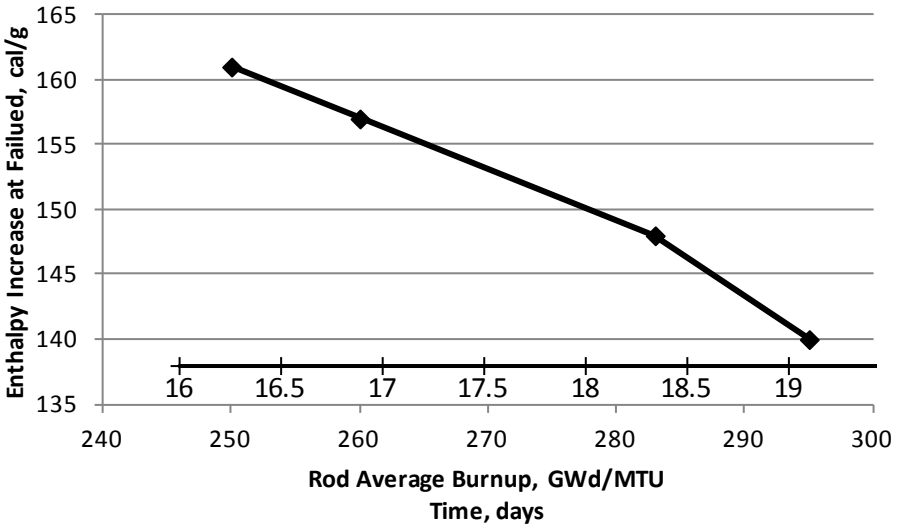

Figure 3.10. Westinghouse 17x17 Design PCMI Failure Threshold (FRAPCON/FRAPTRAN calculated) versus Time (full power days) and Rod Average Burnup (GWd/MTU)

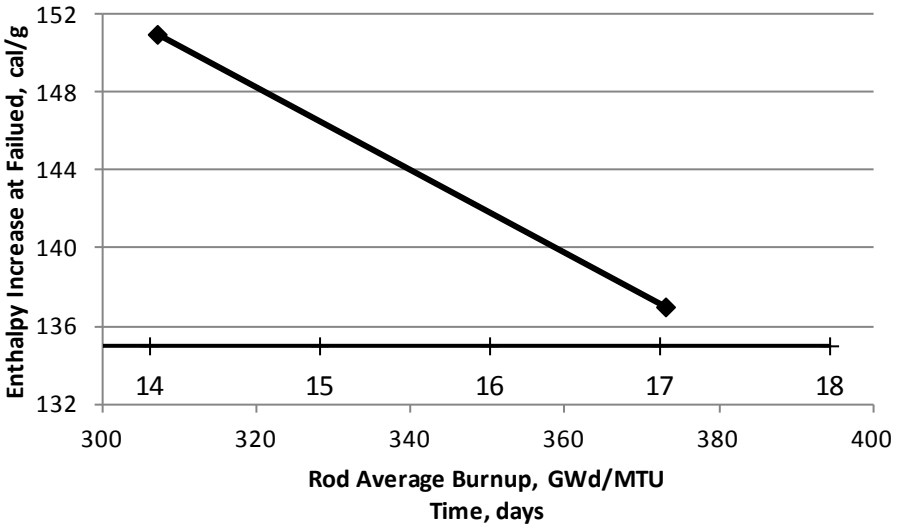

Figure 3.11. Combustion Engineering 14x14 Design PCMI Failure Threshold (FRAPCON/FRAPTRAN calculated) versus Time (full power days) and Rod Average Burnup (GWd/MTU)

3.9 Oxide Spallation Effects

Alvis et al. (2010) has concluded that the rodlets from the CABRI tests that had spalled oxide and localized hydride blisters failed at a lower enthalpy level than those rods with no oxide spallation. The oxide spallation during the base irradiation (normal operation) results in a cooler spot on the cladding that results in hydrogen diffusing to the spalled oxide location resulting in a localized area of hydrides that penetrates the cladding thickness more than non-spalled areas. This lower threshold may be possible because we know that the hydrides are the initiating point for cladding cracking such that a thicker

hydride layer can result in a larger crack length. The three CABRI rods with oxide spallation were CABRI/RepNa1 (652 wppm/13 cal/g), CABRI/RepNa8 (776 wppm/61 cal/g), and CABRI/RepNa10 (574 wppm/64 cal/g). CABRI/RepNa1 has been eliminated from the curve fit data as discussed in Section 3.3. An LSQ fit of the failed data without the CABRI/Na8 and CABRI/Na10 data points was performed and compared to the fit of all the data discussed in Section 3.10.

This LSQ fit without the two rodlets with oxide spallation is shown in Figure 3.12 along with the fit with these two rodlets included for comparison. Figure 3.12 demonstrates that the two fits result in nearly the same failure threshold with the biggest difference at higher excess hydrogen levels, e.g., the difference at 600 wppm is approximately 3 cal/g and at 750 wppm is approximately 4 cal/g. The standard deviation without the two spalled rodlets included in the LSQ fit is approximately 16.4 cal/g and with the two spalled rods included it is approximately 16.9 cal/g such that the uncertainties are also nearly identical. Therefore, the decision was made to include the two CABRI rodlets with oxide spallation, CABRI/Na8 and CABRI/Na10.

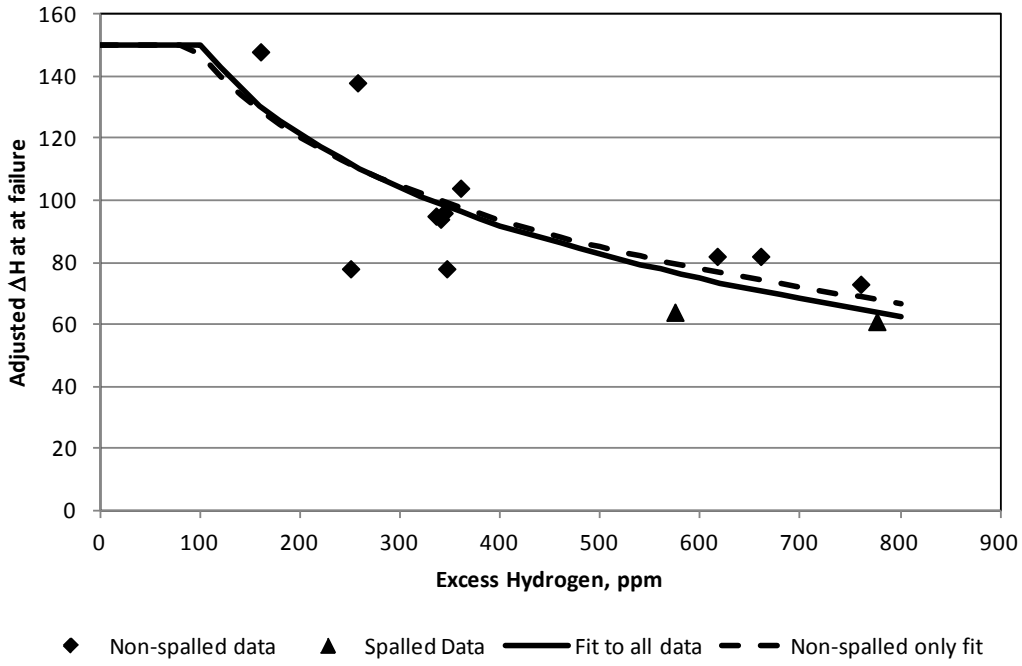

Figure 3.12. Least Squares Fit With and Without Spalled CWSRA Failed Test Data at HZP using a Natural Log Function

3.10 Development of the "Best Estimate" PWR "Hot" PCMI Failure Threshold for CWSRA Cladding

The PWR failure threshold is not only applicable to RIA events starting at HZP conditions based on the data at essentially HZP but it is also applicable to RIAs starting at an initial power greater than zero with the primary coolant "hot," therefore, this PWR failure threshold is referred to as for "hot" initial conditions.

The development of the best-estimate PWR hot failure threshold involves performing a LSQ regression fit using a natural log function of cladding excess hydrogen in the failed RIA test data for rodlets with CWSRA cladding in Figure 3.6 (cold tests adjusted upward by 18 cal/g per discussion in Section 3.3). Figure 3.13 shows the LSQ curve fit to these data in terms of excess hydrogen. This curve has a standard deviation of 16.9 cal/g and $R^2 = 0.61$ ($R^2 = 1.0$ means a perfect fit, all data agree with correlation). The resulting LSQ best-estimate fit in terms of enthalpy change at PCMI failure as a function of excess hydrogen is represented by the following relationship:

$$\Delta H_{fail} = 345 - 42.3\ln(H_{ex}) \tag{3}$$

where ΔH_{fail} = Enthalpy increase at failure, cal/g
H_{ex} = Cladding excess hydrogen, wppm.

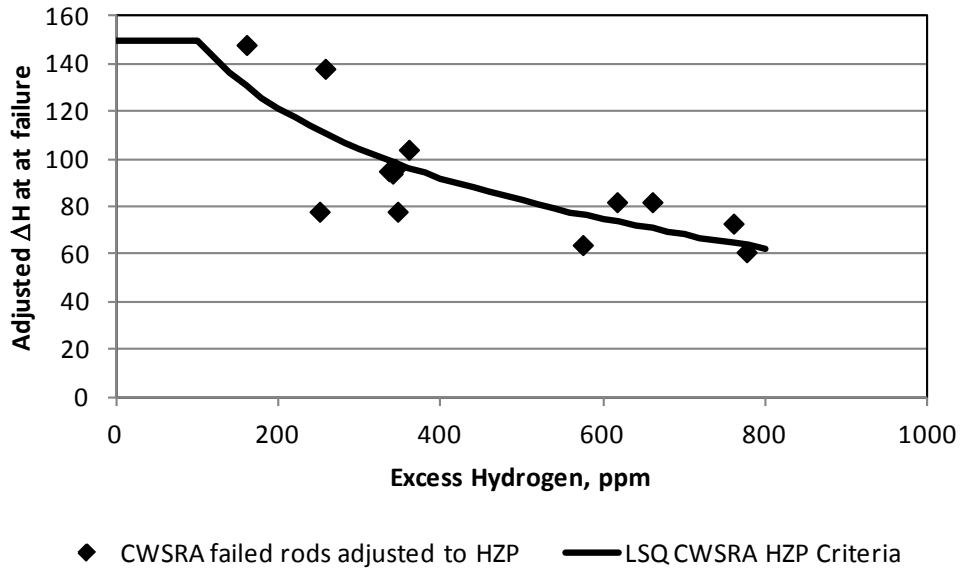

Figure 3.13. LSQ Fit to Failed RIA CWRSA Test Data at HZP (cold tests adjusted upward by 18 cal/g) with a Natural Log Function

As noted in Section 2, (discussing the data used for this derivation of the PWR CWSRA failure threshold), some of the failed NSRR rods with CWSRA cladding have recently had their total peak enthalpy deposited revised (Udagawa et al. 2011), which may change the failure enthalpies for these rods. The change in total peak enthalpy is not large for most of the failed rodlets, but two increased significantly: HBO1 increased from 73 cal/g (306 J/g) to 124 cal/g (518 J/g) and TK2 from 107 cal/g (448 J/g) to 163 cal/g (683 J/g). The VA3 rodlet also increased to a lesser amount from 108 cal/g (454 J/g) to 123 cal/g (515 J/g). The BZ2 failed rodlet total peak enthalpy decreased from 154 cal/g (644 J/g) to 130 cal/g (582 J/g). These changes in total deposited enthalpy will most likely change the failure enthalpies for these rods, particularly, if the change in failure enthalpy is proportional to the change in total peak enthalpy.

A refit of the PWR CWSRA failure threshold has been performed using the revised total peak enthalpies reported by Udagawa et al. (2011) assuming that there is a direct proportionality between the

change in failure enthalpy and total enthalpy deposited developed in Section 3. The assumption of direct proportionality would give the highest revised failure enthalpy and, therefore, is likely the upper limit on revised values, based on the revised total enthalpies. The revised PWR CWSRA delta failure enthalpies for HZP, assuming that they are directly proportional to the change in total enthalpy, were changed from 78 (60 + 18) to 122 cal/g (124/73 * 60 + 20) for HBO1, from 78 (60 + 18) to 111 cal/g (163/107 * 60 + 20) for TK2, from 82 to 93 cal/g (123/108 * 82) for VA3 and from 148 (130 + 18) to 130 cal/g (130/154 * 130 + 20) for BZ2 at HZP. It is also noted that the adjustment of VA3 (hot) from 82 to 93 cal/g increases the delta cold-versus-hot difference with VA1 (cold) increases to approximately 29 cal/g. However, the cold-versus-hot difference for the other cold/hot data pair of BZ1/RepNa7 remains at 20 cal/g. For conservatism we would maintain a cold-versus-hot adjustment of 20 cal/g even if the NSRR adjustment for failure enthalpy is proportional to the total enthalpy values provided by Udagawa et al. (2011). Therefore, cold rod data were increased by 20 cal/g to account for HZP conditions of a limiting PWR RIA event for the LSQ fit. The resulting LSQ fit based on the assumption of revised total enthalpy values by Udagawa et. al. (2011) is represented by the following relationship:

$$\Delta H_{fail} = 352.1 - 42.4 \ln\left(H_{ex}\right) \tag{4}$$

where ΔH_{fail} and H_{ex} remain as defined above.

This failure threshold in Equation 4 increased the PWR failure threshold by approximately 6.4 cal/g at 100 wppm of excess hydrogen and 6.2 cal/g at 800 wppm from that in Equation 3 above, the R^2 improves from 0.61 to 0.73. Therefore, the difference is relatively small and well within the uncertainty of the data.

This evaluation has elected to use the failure enthalpy criteria in Equation 3 rather than Equation 4 because it is unclear how the latest changes to peak total enthalpy in the NSRR data as given by Udagawa et al. (2011) will change the failure enthalpies. In addition, the possible change in the failure criterion is well within the uncertainty of the data (Section 2.1) and Equation 3 is the more conservative threshold.

The maximum enthalpy increase for the failure threshold at low hydrogen (<100 wppm) is assumed to be 150 cal/g which is the same as in the Appendix B of SRP 4.2 (NRC 2007) and NRC 2004 for PWRs from HZP where the failure mechanism is ballooning and rupture. The LSQ failure curve intersects the 150 cal/g failure threshold at approximately 100 wppm excess hydrogen. The resulting LSQ curve then becomes:

$$\begin{aligned} \Delta H_{fail} &= 150 && H_{ex} \le 100 wppm \\ \Delta H_{fail} &= 345 - 42.3 \ln\left(H_{ex}\right) && 100 wppm < H_{ex} \le 800 wppm \end{aligned} \tag{5}$$

The residuals (measured-minus-predicted) from the LSQ fit have been plotted versus burnup and pulse width in Figures 3.14 and 3.15, respectively, to determine if there might be a dependence on either of these variables. The residual plot in Figure 3.14 demonstrates that there might be a dependence with burnup that shows a negative slope and a poor R^2 value equal to 0.21. This negative slope will result in a higher failure threshold for higher burnup fuel if the hydrogen level remains constant. The negative slope with burnup is difficult to explain unless there is increased compliance (softening) of the fuel with burnup that has not been demonstrated experimentally. This dependence with burnup may not be real because of

the poor R^2 value, the small amount of data, the natural uncertainty (scatter in the data), and dependence upon one datum. The weak burnup dependence observed in Figure 3.14 is primarily because of one test datum (NSRR/TK2) that provides a significantly lower threshold than the other data near this hydrogen level. When this test datum is removed the negative slope is significantly reduced by nearly a factor of 2 and R^2 is only 0.13. Therefore, a burnup dependence is not included in the PWR PCMI failure threshold for HZP.

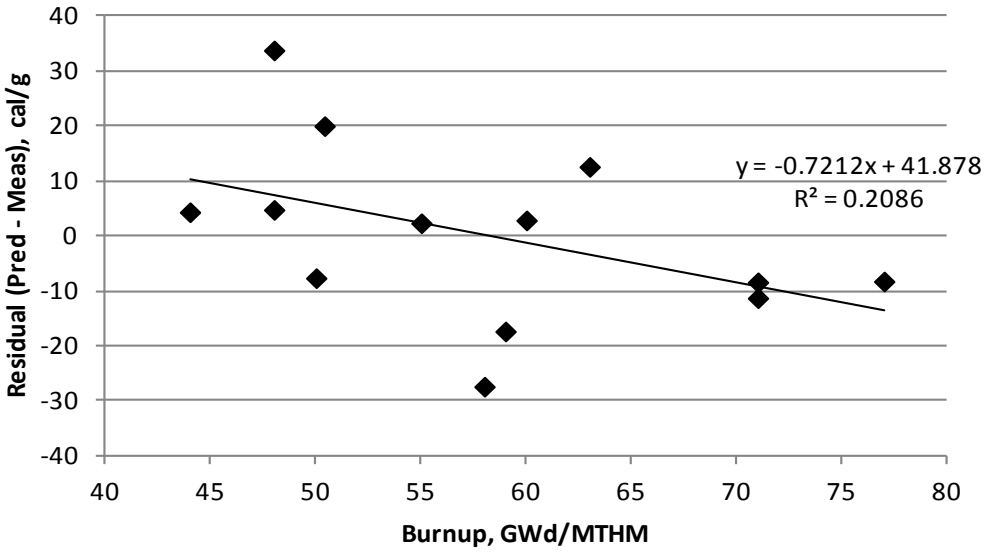

Figure 3.14. Residuals from Natural Log Least Squares Fit of CWRSA Hot Data versus Burnup (GWd/MTU)

Examination of the residual plot in Figure 3.15 and discussion in Section 3.7 demonstrate that there is no dependence on pulse width. Therefore, it is concluded that no burnup or pulse width effect will be included in the CWSRA failure threshold. It is proposed that the fit provided in Figure 3.13 and Equation 3 represents the best estimate failure threshold for CWSRA HZP.

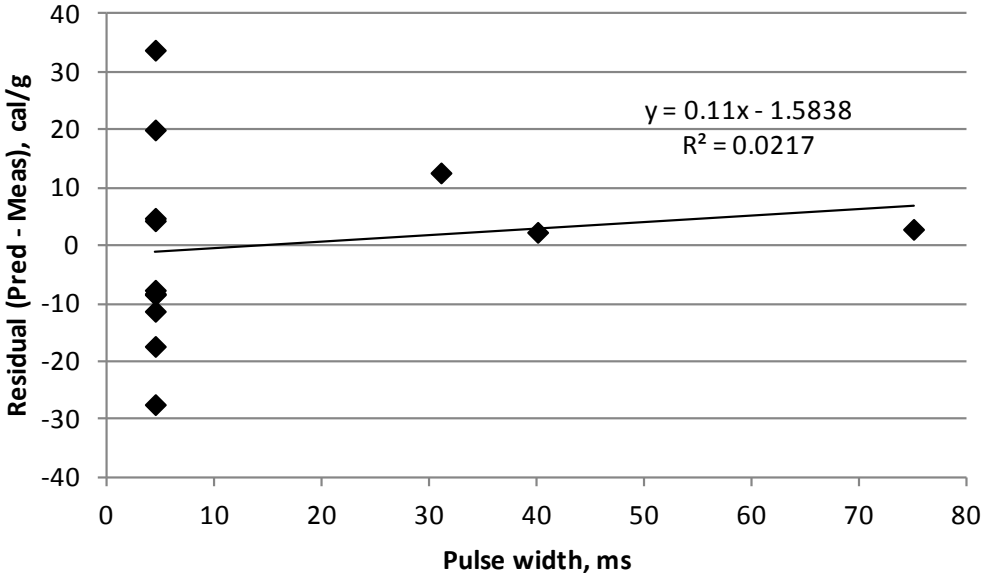

Figure 3.15. Residuals from Natural Log Least Squares Fit of CWRSA Hot versus Pulse Width (ms)

The proposed best-estimate CWSRA HZP failure threshold from the LSQ fit as a function of excess hydrogen (Equation 3) predicts a lower PCMI failure threshold than measured in 6 of 14 failed rods (43 percent) and predicts failure in 7 of 30 rods that did not fail (Figure 3.16). If the best estimate LSQ is biased down by 16.8 cal/g (1 standard deviation it will predict a lower failure threshold than measured in 11 of 13 failed rods (84 percent). If it is biased down by 33.8 cal/g, it will predict a lower failure threshold than measured in 13 of 13 failed rods. Note that those failed rods with measured delta enthalpies greater than 132 cal/g may have failed because of ballooning and rupture.

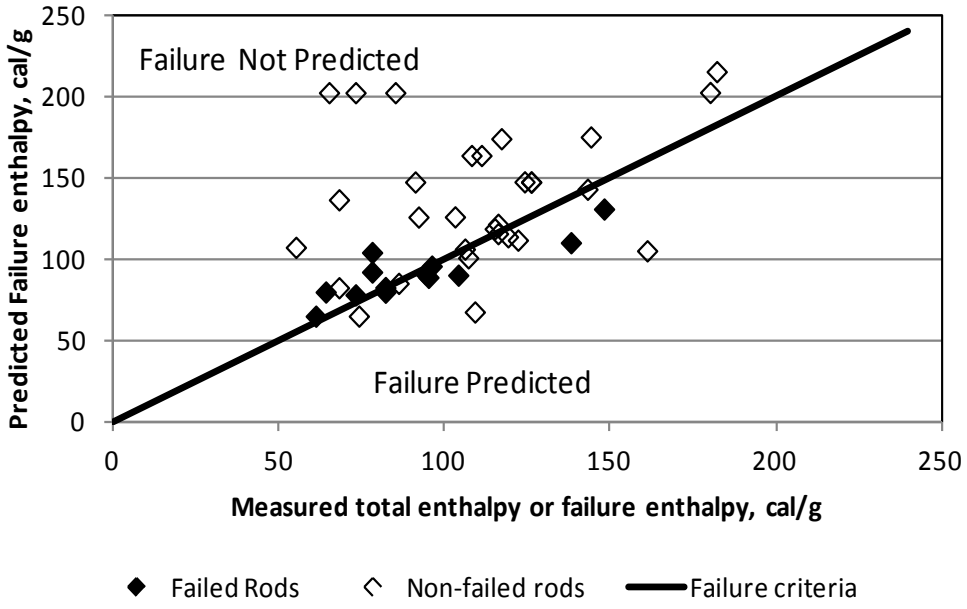

Figure 3.16. Predicted PCMI Failure Delta Enthalpy versus Measured Total Delta Deposited or Failure Enthalpy for CWSRA Non-failed and Failed Tests, Respectively, at HZP

An LSQ regression fit has also been performed with and without the MOX data as a check on whether the conclusion in Section 3.6 that the MOX failure data were similar to the UO_2 data. These LSQ fits are shown in Figure 3.17 and demonstrate the fits with and without the MOX data are very similar. In addition, the standard deviation of the LSQ fit with the MOX data included with the UO_2 data is smaller than the LSQ fit without the MOX (only UO_2) data, i.e., $\sigma = 16.9$ with MOX and $\sigma = 18.2$ with only UO_2. This confirms the previous conclusion that there is no significant difference in the MOX and UO_2 failure data.

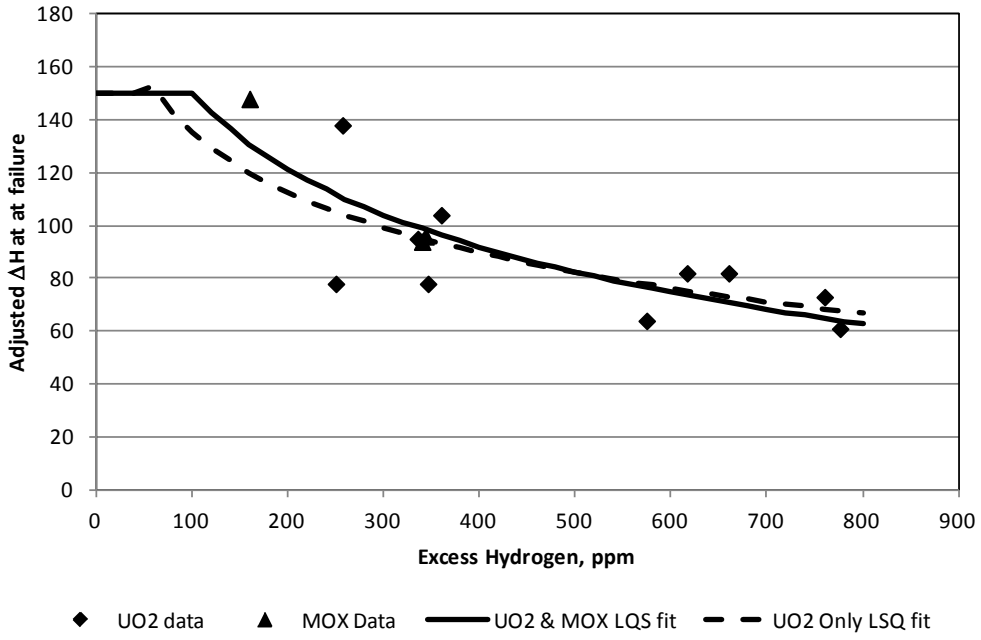

Figure 3.17. Least Squares Fit With and Without MOX CWSRA Failed Test Data at HZP Using a Natural Log Function

A comparison of the LSQ fit to the PWR failure threshold (for CWSRA cladding) proposed in Appendix B of SRP 4.2 (NRC 2007) versus excess hydrogen is provided in Figure 3.18 with error bars for the uncertainty in enthalpy at failure and excess hydrogen of the data. For those rodlets tested under hot conditions the failure delta enthalpy uncertainty (error bar) is assumed to be ± 10 cal/g (Section 2.1) while those rodlets adjusted for cold to hot conditions the uncertainty is assumed to be ± 14 cal/g (Section 3.3). Note that the failure enthalpy (vertical) error bars for TK2 and HBO1 at 250 wppm and 346 wppm excess hydrogen, respectively, are significantly higher than the other data on the plus side. This is because as discussed in this section, and in Section 2, a recent paper by Udagawa et al. (2011) has increased the total enthalpy deposited in these two rods by ≥ 50 percent, the impact on failure enthalpy increase has not been estimated at this time but they are likely to increase. The error bars for the failure enthalpies for VA3 and BZ2 are also increased, based on the revised total enthalpies deposited in these two rods by Udagawa et al. (2011) as discussed in this section and in Section 2.

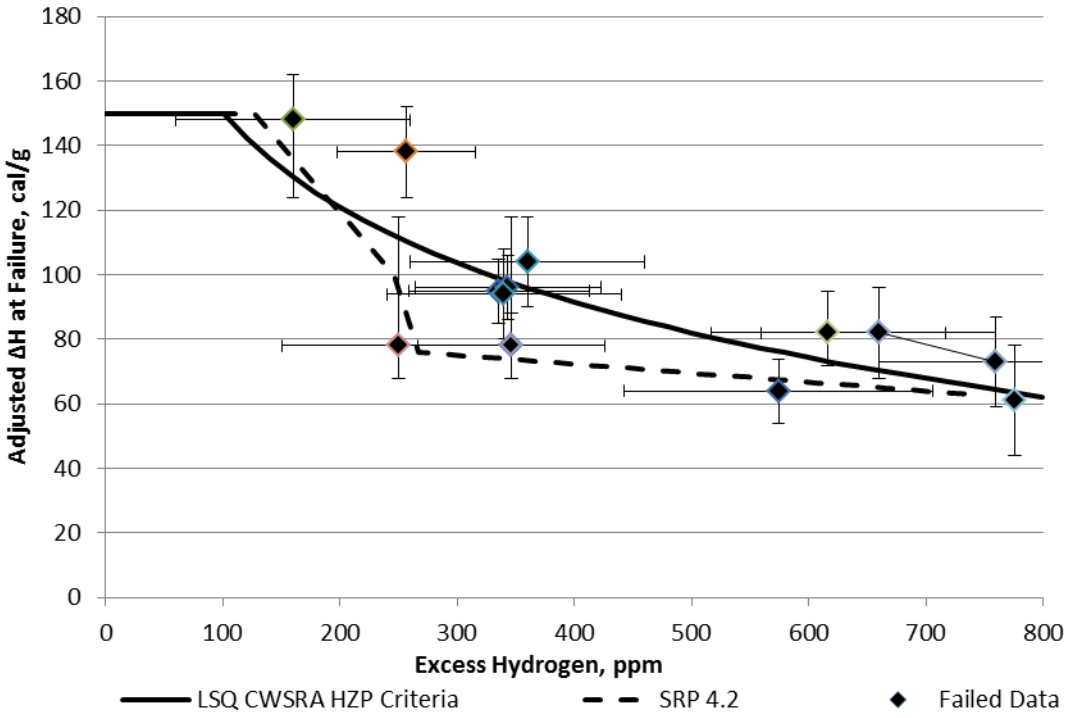

Figure 3.18. Comparison of LSQ Fit Failure Threshold Curve to the Appendix B of SRP 4.2 (NRC 2007) Failure Threshold for CWSRA HZP Event in Terms of Excess Hydrogen with Error Bars for Uncertainty in Data

The original PCMI failure threshold in the SRP was plotted versus the ratio of oxide thickness to wall thickness, this was converted to excess hydrogen assuming a 17x17 design with Zry-4 cladding, a 0.594-mm wall thickness, and a diameter of 9.5 mm and a hydrogen pickup fraction of 0.15 (from FRAPCON-3.4). This comparison demonstrates a similar relationship between these two proposed failure PWR PCMI thresholds for HZP. The LSQ fit decreases at a lower excess hydrogen level than the SRP (100 wppm versus 126 wppm) providing a slightly lower failure enthalpy between 100 wppm and 180 wppm while above 200 wppm to 600 wppm, the SRP failure threshold becomes lower with the two asymptoting to a similar failure threshold beyond 600 wppm. The biggest differences between the least squares fit and the SRP are at 306 wppm, a 29-cal/g difference where there are four test data. It is difficult to determine whether the LSQ or SRP failure threshold provides the better fit at low excess hydrogen levels (< 200 wppm) because only one failed point exists. The LSQ failure threshold provides a better fit above 300 wppm excess hydrogen because the SRP is more conservative in this range. For example, if the SRP failure threshold is lowered by 5 cal/g, it would bound 12 of the 13 failed data points. The SRP PWR failure threshold is expressed by the following relationships:

$$\begin{aligned} \Delta H_{fail} &= 150 && H_{ex} \le 126 wppm \\ \Delta H_{fail} &= 150 - 0.4177\left(H_{ex} - 126\right) && 126\,ppm < H_{ex} \le 306 wppm \\ \Delta H_{fail} &= 75 - 0.02785\left(H_{ex} - 306\right) && 306\,ppm < H_{ex} \le 800 wppm \end{aligned} \quad (6)$$

The standard deviation of the SRP failure threshold to the failure data is 20.8 cal/g versus 16.8 cal/g for the LSQ. The major reason for the larger standard deviation for the SRP threshold is the overprediction of the NSRR/TK2 test data that had a measured failure at 78 cal/g (250 wppm hydrogen), while the SRP predicted value was 126 cal/g, and the LSQ threshold criteria predicted 111 cal/g, which is also a significant overprediction, but is less than the SRP. This difference is evident in Figure 3.19 where predicted versus measured is provided for both the SRP and LSQ failure thresholds. As noted in this section and Section 2 the TK2 measured failure of 78 cal/g maybe revised upward based on recently revised total enthalpy values that increased by approximately 50 percent based on Udagawa et al. (2011) paper. If the TK2 failure enthalpy were increased by 50 percent this would place this data point nearly on the LSQ failure threshold curve and just above the SRP curve.

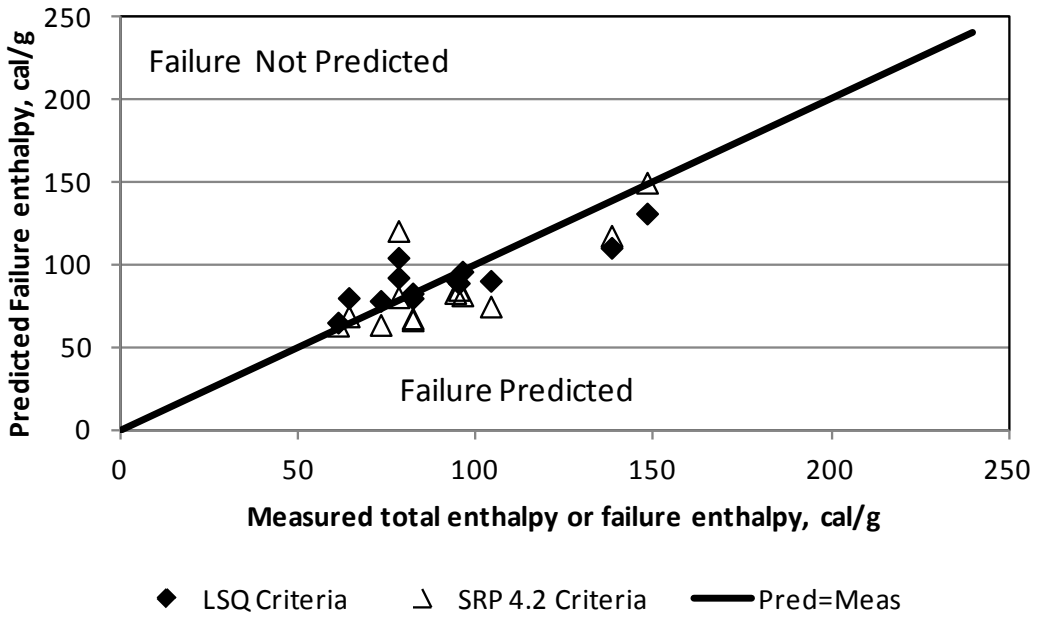

Figure 3.19. Predicted Versus Measured Failure Delta Enthalpy for Failed Data for the LSQ and SRP 4.2 Failure Thresholds at HZP for SRA Cladding

3.11 Development of the PWR "Hot" PCMI Failure Threshold for RXA Cladding

Currently, the only RXA cladding alloy approved for use in U.S. PWRs is M5™. Since none of the RIA tests with M5™ cladding failed, RXA data from the NSRR (Zry-2 cladding) will be used to develop the RXA PCMI failure threshold for HZP. The NSRR data are adjusted up by 18 cal/g (observed difference between hot and cold conditions).

An LSQ fit made using the NSRR data (high hydrogen > 100 wppm) that was adjusted upward by 18 cal/g for HZP, is shown in Figure 3.20. The adjustment of 18 cal/g accounts for temperature effects on cladding ductility for the PCMI failure mechanism for the cold (more brittle cladding) NSRR data. The resulting best estimate fit in terms of enthalpy change as a function of excess hydrogen is represented by the following relationship

$$\Delta H_{fail} = 321 - 44.2 \ln(H_{ex}) \quad (7)$$

where ΔH_{fail} = enthalpy increase from zero power conditions at failure, cal/g
H_{ex} = cladding excess hydrogen, wppm

This correlation has a standard deviation of 6.7 cal/g relative to the data but it should be noted that this value is only based on a small database and may be higher.

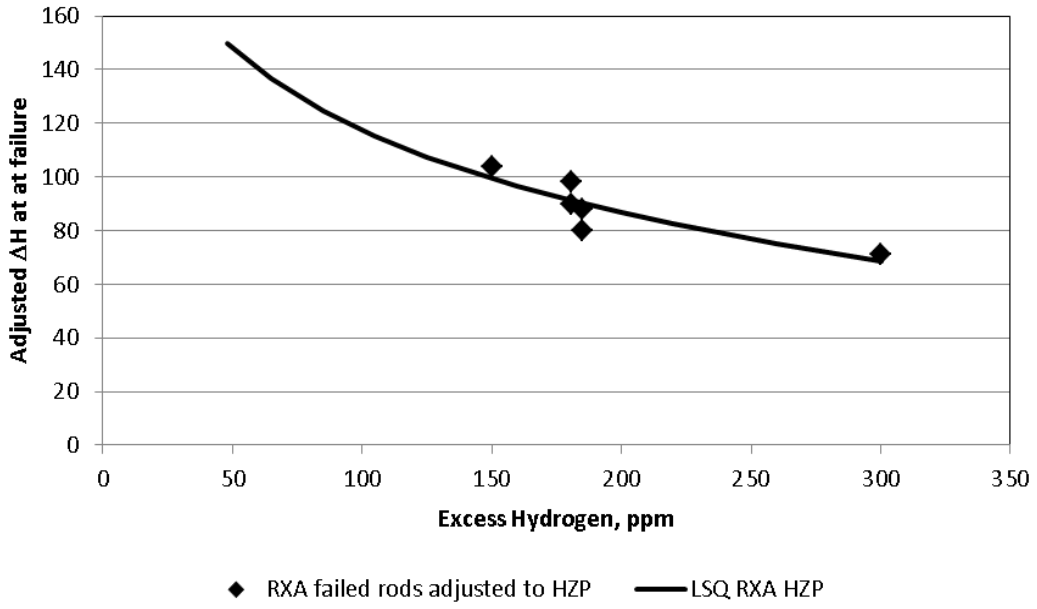

Figure 3.20. Least Squares Fit with a Natural Log Function to Failed NSRR RXA Test Data Adjusted Upward by 18 cal/g for Initial HZP Conditions for M5™

At low excess hydrogen levels where failure is because of cladding ballooning and rupture, the failure enthalpy is kept constant at 150.0 cal/g for RXA cladding as assumed in the Appendix B of SRP 4.2 (NRC 2007) and NRC 2004 for PWRs from HZP. The level where the LSQ fit intersects the 150 cal/g threshold is at 48 wppm of excess hydrogen. This threshold is assumed to be constant versus excess hydrogen because as noted, the ballooning and rupture mechanism is only dependent on total enthalpy deposited and not because of ductility loss and, therefore, not dependent on excess hydrogen. The LSQ failure threshold curve to be applied to M5™ for PCMI above 48 wppm that also accounts for the ballooning and rupture threshold below 48 wppm excess hydrogen is represented by the following equations:

$$\begin{aligned} \Delta H_{fail} &= 150 && H_{ex} \le 48 wppm \\ \Delta H_{fail} &= 321 - 44.2 \ln(H_{ex}) && 48 wppm < H_{ex} \le 300 wppm \end{aligned} \quad (8)$$

A comparison of the LSQ fit to the BWR RXA failure threshold proposed in Appendix B of SRP 4.2 (NRC 2007) in terms of excess hydrogen is provided in Figure 3.21 for HZP conditions. The BWR RXA failure threshold curve in the SRP is for CZP, therefore, the PCMI portion of the SRP CZP failure threshold curve, which is at excess hydrogen levels greater than 75 wppm in Figure 4.5 is adjusted

upward by 18 cal/g to account for HZP conditions in Figure 3.21. The assumed delta enthalpy threshold for ballooning and rupture of 150 cal/g has not been adjusted upward by 18 cal/g because this failure mechanism is not ductility dependent, as is the PCMI failure mechanism at higher excess hydrogen levels. Also, included in Figure 3.21 are error bars (one standard deviation) on the delta failure enthalpy and excess hydrogen of the data as discussed in Section 2.1. The SRP RXA failure threshold for HZP to be applied to M5™ is represented by the following equations:

$$\begin{aligned} \Delta H_{fail} &= 150 && H_{ex} \le 75\,ppm \\ \Delta H_{fail} &= 150 - 0.96\left(H_{ex} - 75\right) && 75\,ppm < H_{ex} \le 150\,ppm \\ \Delta H_{fail} &= 78 - 0.06667\left(H_{ex} - 150\right) && 150\,ppm < H_{ex} \le 300\,ppm \end{aligned} \tag{9}$$

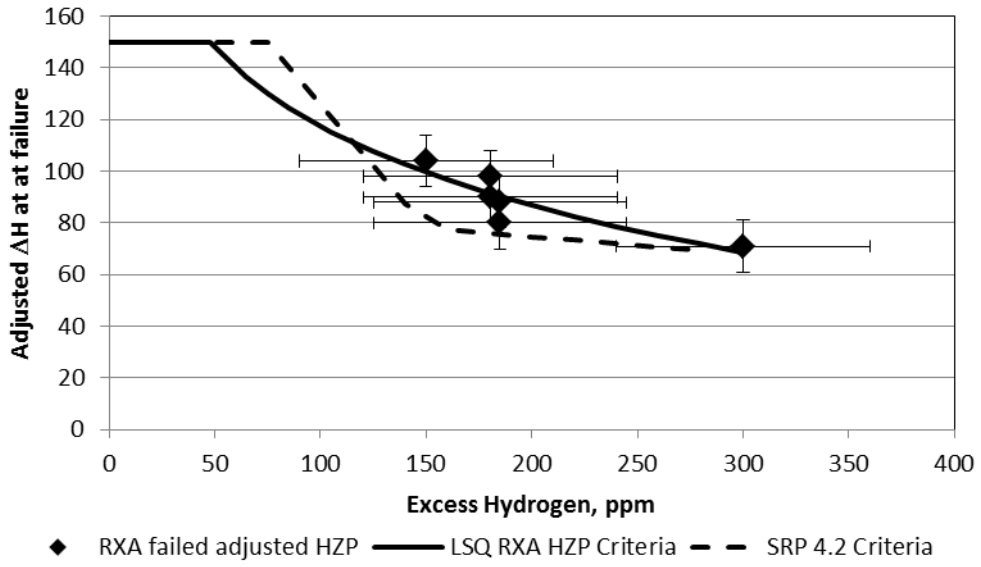

Figure 3.21. Comparison of Least Squares RXA fit to SRP 4.2 BWR (RXA) Threshold Adjusted Upward by 18 cal/g for HZP with NSRR RXA Data Also Adjusted for HZP for M5™ with Error Bars for Uncertainty in Data

The BWR RXA failure threshold curve in the SRP for PCMI and CZP was plotted in terms of excess hydrogen unlike the PWR PCMI threshold curve from the SRP. This comparison demonstrates the LSQ failure threshold is more conservative than the SRP for HZP between 48 wppm and 105 wppm where there are no failure data. Between 125 wppm and 270 wppm, the SRP failure threshold is more conservative (lower) with a maximum difference of 20 cal/g at 150 wppm, then asymptoting to similar values above 270 wppm. It should be noted that the shape (slope) of the failure threshold curve between 48 wppm and 150 wppm excess hydrogen is speculative because no data exist in this range. The LSQ failure threshold provides a better fit between 150 wppm and 200 wppm because the SRP failure threshold provides a lower bound to the data. It should be noted that both thresholds are within one standard deviation of the failure data. The proposed best estimate RXA HZP failure threshold from the LSQ fit as a function of excess hydrogen (Equations 7 and 8) for PCMI (> 48 wppm of hydrogen) predicts a lower failure threshold than measured in 3 of 6 failed rods (50 percent) by PCMI and predicts failure in 4 (LS1, FK1, FK3, and FK4) of 17 rods that did not fail (Figure 3.22). If the LSQ failure threshold were biased down by 13 cal/g it would equal or bound all of the RXA data.

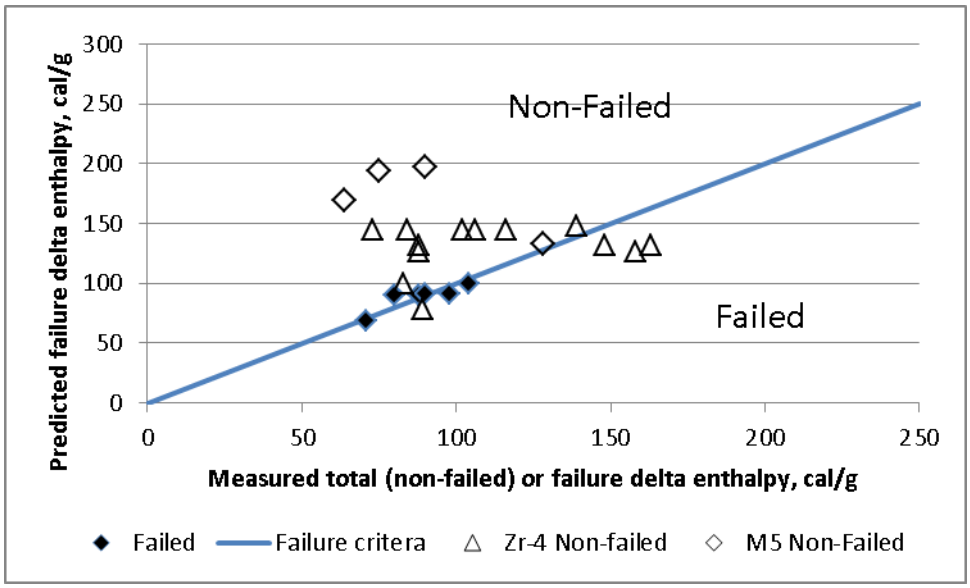

Figure 3.22. Predicted PCMI Failure Delta Enthalpy versus Measured Total Delta Deposited or Measured Failure Enthalpy for RXA Non-failed and Failed Tests, Respectively, at HZP

The failure threshold for RXA cladding (Figure 3.21) is lower than for CWSRA cladding (Figure 3.18) for similar excess hydrogen levels. The lower threshold for RXA cladding is because the hydride platelets precipitate in a more random orientation. This randomness results in some of these hydrides being orientated in the radial direction where crack initiation becomes more likely when a hoop tensile stress (perpendicular to the hydride platelet) is experienced by the RXA cladding which is the stress orientation for PCMI during a RIA event. This random orientation of hydrides is believed to be because of the random orientation of the RXA grain structure because the hydrides prefer precipitation on the grain boundaries. This randomness of hydride orientation in RXA cladding and its impact on PCMI failure are also discussed in the NEA (2010) report. The CWSRA material has a grain structure that is aligned in the circumferential direction (direction of hoop stress) which is the direction of (parallel to) the hydride platelets. The PWR M5™ cladding is RXA with a similar grain structure as Zry-2 RXA; therefore, the hydride orientation in M5™ will likely have some radial hydrides similar to Zry-2 RXA.

It should be noted that even though the threshold is lower for M5 RXA cladding at equivalent hydrogen levels, the failure threshold is generally higher than for CWSRA cladding (also depends on plant duty) at equivalent burnup levels because of the low pickup of hydrogen (< 200 wppm total hydrogen) for M5.

3.12 PWR "Hot" PCMI Failure Threshold for Partially Recrystallized Cladding

Westinghouse has recently introduced a low tin ZIRLO™ (Optimized ZIRLO™) for PWR application that does not have a CWSRA heat treatment but is instead pRXA. No mechanical property test data are available, nor are there data on the hydride orientation of Optimized ZIRLO™ found in the open literature. Therefore, no conclusions can be made as to the applicability of the failure thresholds

presented in this report to Optimized ZIRLO™. The M5™ correlation should be used unless it can be demonstrated that the orientation and distribution of hydrides in irradiated Optimized ZIRLO™ is similar to that of standard ZIRLO™. Also, mechanical test data (including measured uniform strains) from the irradiated new cladding that demonstrates similar behavior to either CWSRA or RXA alloys that are currently approved and described above, must be provided to the U.S. Nuclear Regulatory Commission (NRC). If this is demonstrated applicable to CWSRA, the CWSRA failure threshold may be used for Optimized ZIRLO™.

For new cladding alloys not discussed here, the applicant should either present mechanical test data (including measured uniform strains) from the irradiated new cladding that demonstrates similar or bounding behavior to either CWSRA or RXA alloys that are currently approved and described above, or derive a new correlation based on in-reactor or out-of-reactor tests that simulate at service conditions similar to those for a RIA with the new alloy. The mechanical test methodology used to measure mechanical properties should demonstrate that it is applicable to failure strains from the CABRI and NSRR tests. It should also demonstrate that the hydride morphology in the irradiated new alloy is similar to one of the alloys described above if a current correlation is to be applied for the new alloy.

3.13 Uncertainty in PWR Failure Thresholds

The cold-to-hot adjustment for most of the NSRR data has a significant impact on the PWR failure thresholds. Because it is difficult to estimate the uncertainty (there are only two hot/cold data pairs) this may be a source of significant uncertainty in the PWR failure thresholds, Section 3.3 has estimated the uncertainty to be ± 14 cal/g.

The uncertainty in the PCMI failure threshold for CWSRA cladding is greatest below 300 wppm of excess hydrogen because only three data points exist because of PCMI failure. There are four BIGR data points that failed below 70 wppm excess hydrogen but these likely did not fail because of PCMI. In addition, the failure threshold is not valid above 800 wppm excess hydrogen because no failure data exist above this excess hydrogen level. The uncertainty in this threshold may also be affected because the recent paper by Udagawa et al. (2011) has increased the enthalpy deposited in NSRR rodlets TK2 and HBO1 by approximately 40 to 50 percent, the impact on failure enthalpy has not been estimated at this time but they are likely to increase (as discussed in Sections 2 and 3.10). Section 3.10 evaluates the possible impact of the Udagawa et al. (2011) paper that revised the total enthalpy deposited in some of the NSRR rodlets that will likely increase the NSRR delta failure enthalpies for these rodlets and the maximum possible change in the LSQ failure threshold fit for CWSRA cladding. This LSQ refit based on the possible changes to the NSRR failure data from Udagawa et. al. (2011) shows that the maximum increase in the PCMI failure threshold would be approximately 10 cal/g at 100 wppm and approximately 5 cal/g at 800 wppm excess hydrogen.

The uncertainty in the PCMI failure threshold for RXA cladding is the least between 150 and 200 wppm of excess hydrogen because 5 of the 6 PCMI failure data exist in this range. As the failure threshold deviates from this range the uncertainty becomes greater below 150 wppm and between 200 and 300 wppm of excess hydrogen and is not valid above 300 wppm because of the lack of data.

3.14 PWR “Hot” Limitations

The limitations for application of the PWR HZP failure thresholds (both LSQ and SRP)

- are fuel designs with gap-to-fuel rod diameter ratio (g/d) limited to 0.0147 or larger (impacts threshold prior to hard gap closure at low-to-moderate burnup levels)
- are applicable to Zircaloy-4 CWSRA, ZIRLO™, and M5™ cladding
- include a burnup limit of 75 GWd/MTU peak pellet (based on data)
- are not valid for excess hydrogen above 800 wppm for CWSRA cladding or above 300 wppm for RXA cladding because of the lack of data
- include no fuel additives other than Gd_2O_3, PuO_2, and sintering aids
- are valid for alloys with orientation and distribution of hydrides that are similar to Zry-4, ZIRLO™, or M5™. Mechanical properties must also be similar to one of these alloys based on acceptable mechanical test methods that are demonstrated to be applicable to the RIA test data.

4.0 BWR PCMI Threshold

Both CWSRA and RXA versions of Zry-2 cladding are being used in operating BWRs in the United States. Similar to the PCMI cladding failure thresholds developed for PWR hot conditions, separate CWSRA and RXA failure curves will be developed for BWR cold startup conditions.

Appendix B provides the BWR test data, the measured total hydrogen values are provided when measured values are given (14 of the 21 test data); when values of hydrogen were not measured (7 test data) they are calculated from the fuel rod burnup using the recommended correlation for hydrogen pickup in FRAPCON-3.4 (Geelhood and Beyer 2011). As can be seen from Appendix B there are many fewer data points for BWR RIA test rods with Zircaloy-2 RXA cladding (only 21 total test data with 6 failed tests), these tests are all from NSRR.

In an attempt to increase the number of available RIA tests for RXA material, the BIGR tests (Yegorova et al. 2005a, 2005b) that included test rodlets from VVER rods (PWR) with E-110 cladding were examined. Although E-110 is not a licensed alloy in the United States, it is noted that it has a RXA heat treatment and has an alloy composition similar to M5™ and is expected to behave similarly to the U.S. RXA alloys (M5™ and Zry-2) for a comparable RIA event. The BIGR tests include 12 rodlets tested from CZP (room temperature). Only four of these rodlets failed between 164 cal/g and 188 cal/g, which is in the enthalpy range where ballooning and rupture is believed to be the dominant failure mechanism. These four failed data will not be used to determine a BWR RXA failure threshold for PCMI because they likely did not fail by PCMI.

4.1 Range of BWR Fuel Enthalpy and Hydrogen Levels Tested

Figure 4.1 provides the range of test data from NSRR in terms of peak enthalpy change deposited in the fuel versus excess hydrogen level for both MOX and UO_2 fuel. All but one of these rods have been tested with initial temperatures near room temperature (20°C) that matches the limiting RIA event for commercial BWRs that occurs at CZP. Only one BWR rod had MOX fuel at relatively low excess hydrogen of 60 wppm that did not fail. The BWR rods have been tested up to 145 cal/g peak fuel enthalpy change at 72 wppm excess hydrogen and up to 112 cal/g peak enthalpy change at 300 wppm hydrogen.

The four BIGR test data that failed are also included in Figure 4.1 for information. All four of these data had hydrogen levels of less than 70 wppm with failure enthalpies between 164 cal/g and 188 cal/g such that they most likely failed because of ballooning and rupture and not PCMI. Because of this, these rods were not included in the LSQ fits to determine the PCMI failure thresholds.

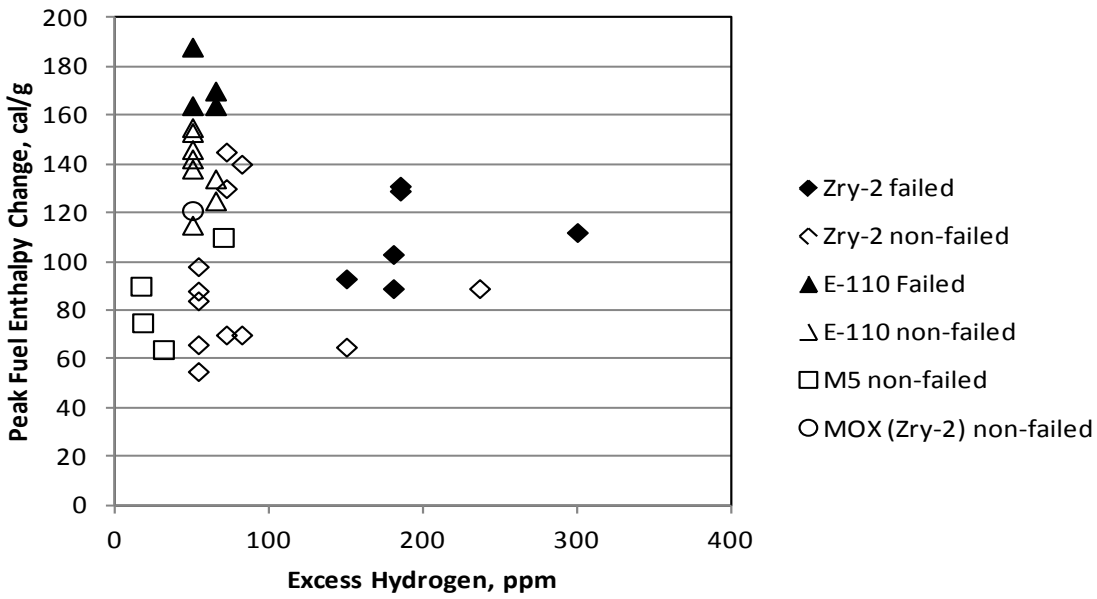

Figure 4.1. Range of Peak Total Enthalpy Change Deposited in Fuel versus Excess Hydrogen for UO_2 and MOX Test Rods with Zry-2, M5™, and E110 RXA Cladding

4.2 Hydrogen, Cold Versus Hot, Cladding Type, MOX, Pulse Width, Initial Gap, and Burnup Effects

Excess hydrogen has a strong effect on PCMI failure threshold for BWR rods at CZP as demonstrated in Figure 4.2 where the failure enthalpy is included for failed rodlets (solid symbols) and total deposited enthalpy in the fuel for non-failed rodlets (open symbols). The decrease in enthalpy with excess hydrogen is at a lower excess hydrogen level than for CWSRA cladding adjusted for comparable CZP conditions. This is most likely because RXA cladding has a more random orientation of hydrides (i.e., some hydrides have radial orientation), while CWSRA cladding has hydrides only in the circumferential direction. Recent ex-reactor mechanical testing on cladding with radial hydrides has shown that the radial hydride length is also important in failure; it is likely that radial hydride density (connectivity of hydrides) is also important. However, neither of these has been measured in the NSRR and CABRI cladding tested, and is rarely measured prior to ex-reactor mechanical testing. Therefore, it is not possible to include these effects in a RIA failure threshold.

Cold-versus-hot effects will be treated in the same manner as for PWRs with the exception that the only hot RXA test (NSRR/LS2 non-failed test) has adjusted the peak fuel enthalpy down by 18 cal/g. The report by Alvis et al. 2010 also has a temperature adjustment for the failure threshold for a BWR CZP RIA. This report suggests that the DBTT for Zr-2 RXA cladding is 80°C to 85°C, based on data that were not presented or referenced. The report further proposes that for a BWR RIA event that initiates near room temperature (CZP) the cladding will be near 85°C or greater by the time PCMI is experienced. As a result the report increases the BWR CZP failure threshold for Zr-2 RXA cladding from the NSRR tests by approximately 22 cal/g at 150 to 200 ppm and by approximately 15 cal/g at 300 ppm assuming the DBTT is 85°C.

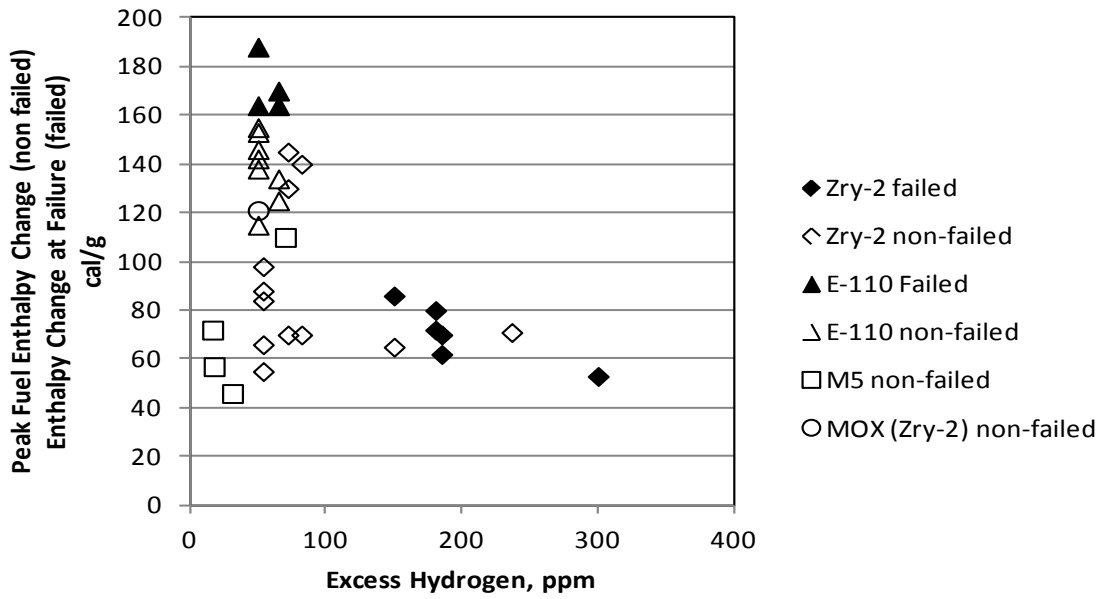

Figure 4.2. Peak Fuel Enthalpy Change at Failure (for failed rods only) versus Excess Hydrogen for All RXA Test Rodlets at CZP Results (solid symbols are failed and open symbols are non-failed test rods), NSRR Hot LS2 Test is Adjusted Down by 18 cal/g

The validity of this adjustment has been examined based on two NSRR test rods with irradiated Zr-2 RXA cladding and open literature DBTT testing of irradiated Zr-2 RXA cladding. The two NSRR BWR test rods were FK10 and FK12 (Zr-2 RXA) tested with initial coolant temperatures of 80°C and 85°C, respectively (NEA 2010). No difference in failure mode was observed in these Zr-2 RXA rods from those tested at 20°C (NEA 2010). The cladding temperatures typically increase only by a small amount for NSRR tests at the failure enthalpy levels for these rods (80 and 72 cal/g) but it is typically equal to or greater than 10°C (NEA 2010). Therefore, the cladding temperatures for FK10 were greater than 90°C and FK12 were greater than 95°C at failure, suggesting that, from these RIA tests, the ductile–to-brittle transition for irradiated Zr-2 RXA is above these temperatures.

A paper by Kubo et al. (2010) has reported a DBTT for irradiated Zr-2 RXA between 250°C and 300°C for plane strain, applicable to PCMI. A paper by Sugiyama et al. (2011) suggests that DBTT is above 200°C for irradiated Zr-2 RXA. Based on the FK10 and FK12 NSRR tests and the Kubo et al. (2010) paper it is concluded that a temperature adjustment at 85°C for a BWR CZP RIA is not justified.

The effect of cladding type (RXA versus CWSRA) will be determined the same as for PWRs with a different threshold for RXA and CWSRA cladding at CZP. As determined from the PWR data, no effect of MOX, pulse width, initial gap size, or burnup will be included in the BWR failure thresholds. These effects could not be evaluated independently from the BWR failed test data because of the much smaller BWR database.

4.3 Development of the BWR CZP PCMI Failure Threshold for RXA Cladding

The development of the best-estimate BWR CZP failure threshold involves performing an LSQ regression fit to the failed RIA test data for rodlets with RXA cladding (NSRR Zry-2). All failed tests are cold tests and were not adjusted. The LSQ curve fit to these data in terms of excess hydrogen is provided in Figure 4.3 and has a standard deviation of 6.7 cal/g and $R^2 = 0.75$ ($R^2 = 1.0$ means a perfect fit, all data agree with correlation). The resulting LSQ best estimate fit in terms of enthalpy change at PCMI failure as a function of excess hydrogen is represented by the following relationship:

$$\Delta H_{fail} = 303 - 44.2 \ln(H_{ex}) \tag{10}$$

where ΔH_{fail} = enthalpy increase from zero power conditions at failure, cal/g
H_{ex} = cladding excess hydrogen, wppm.

The ballooning and rupture threshold at CZP is assumed to be the same as that currently provided in Appendix B of SRP 4.2 (NRC 2007) at a value of 150 cal/g. The LSQ failure threshold curve intersects the 150 cal/g value at 32 cal/g excess hydrogen as shown in Figure 4.3.

The proposed best-estimate RXA CZP failure threshold from the LSQ fit as a function of excess hydrogen (Equations 10 and 11) for PCMI (> 32 wppm of hydrogen) predicts a lower failure threshold than measured in 3 of 6 failed rods (50 percent) by PCMI failure and predicts failure in 4 of 17 rods that did not fail (LS1, FK1, FK3, and FK4), Figure 4.4. If the LSQ failure threshold were biased down by 10 cal/g, it would equal or bound all of the RXA data.

The threshold below 32 wppm is assumed to be constant versus excess hydrogen because as noted previously the ballooning and rupture mechanism is only dependent on total enthalpy deposited and not on ductility loss and, therefore, not dependent on excess hydrogen. The NRC (2004), NEA (2010), and Alvis et al. (2010) came to similar conclusions that below a given hydrogen level the failure mechanism changes from PCMI to cladding ballooning/rupture. The LSQ failure threshold to be applied to RXA Zircaloy-2 that accounts for the ballooning and rupture threshold below and PCMI above 32 wppm excess hydrogen is represented by the following equations:

$$\begin{aligned} \Delta H_{fail} &= 150 && H_{ex} \le 32 wppm \\ \Delta H_{fail} &= 303 - 44.2 \ln(H_{ex}) && 32 wppm < H_{ex} \le 300 wppm \end{aligned} \tag{11}$$

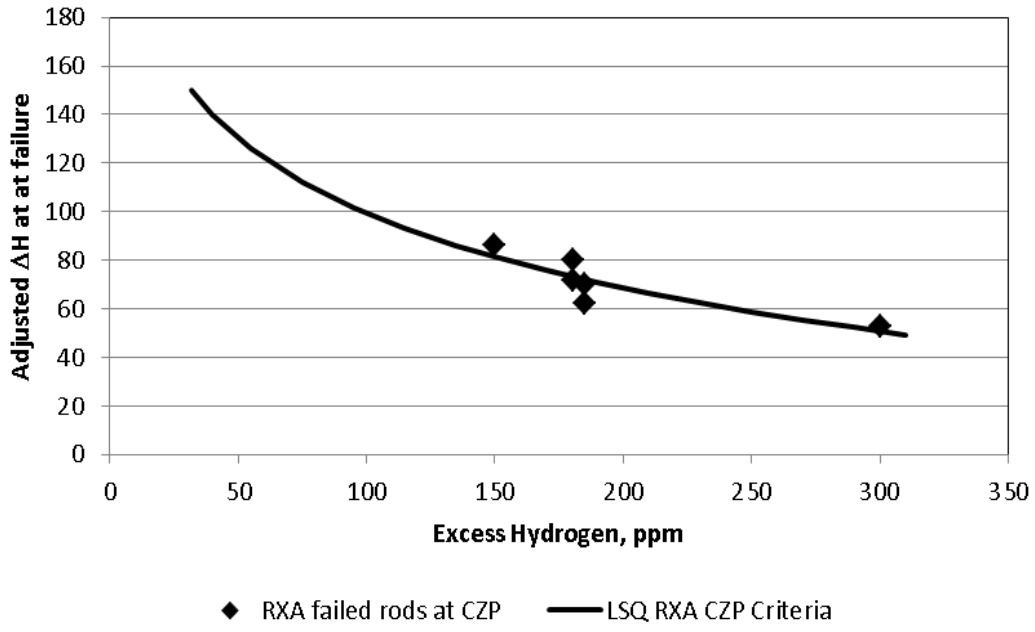

Figure 4.3. Least Squares Fit with a Natural Log Function to Failed NSRR RXA Test Data at CZP

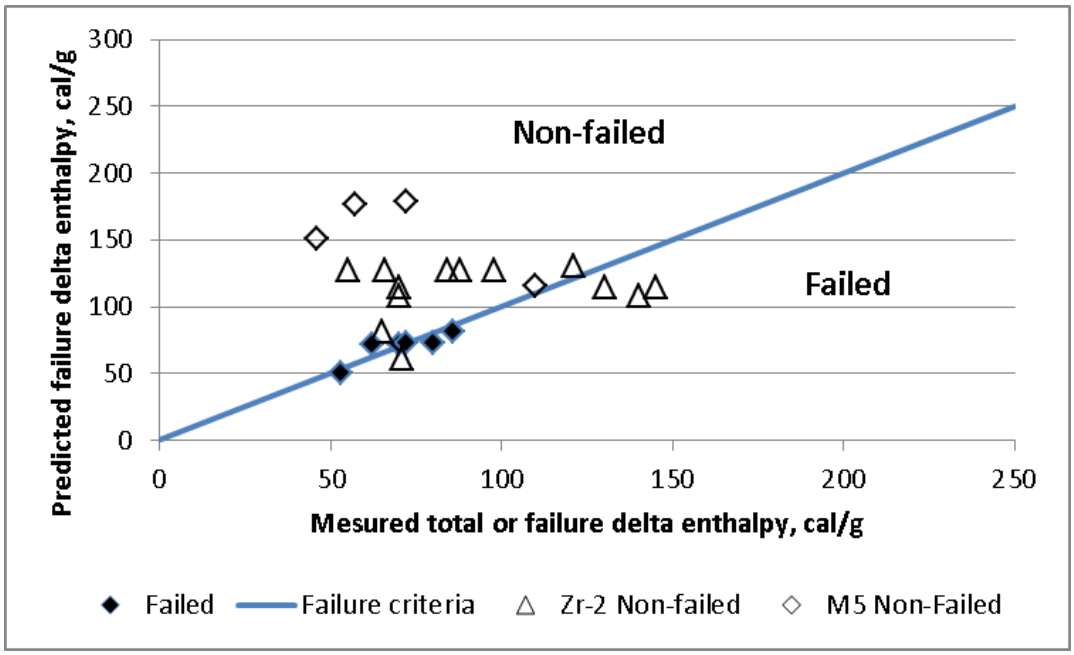

Figure 4.4. Predicted PCMI Failure Delta Enthalpy versus Measured Total Delta Deposited or Failure Enthalpy for RXA Non-failed and Failed Tests, Respectively, at CZP

A comparison of the LSQ fit to the BWR RXA failure threshold proposed in Appendix B of SRP 4.2 (NRC 2007) in terms of excess hydrogen is provided in Figure 4.5 for CZP. Also, included in Figure 4.5 are error bars (one standard deviation) on the delta failure enthalpy and excess hydrogen as discussed in Section 2.1. The SRP RXA failure threshold applicable to CZP is represented by the following equations:

$$\begin{aligned} \Delta H_{fail} &= 150 && H_{ex} \le 75\,ppm \\ \Delta H_{fail} &= 150 - 1.2\left(H_{ex} - 75\right) && 75\,ppm < H_{ex} \le 150\,ppm \\ \Delta H_{fail} &= 60 - 0.06667\left(H_{ex} - 150\right) && 150\,ppm < H_{ex} \le 300\,ppm \end{aligned} \quad (12)$$

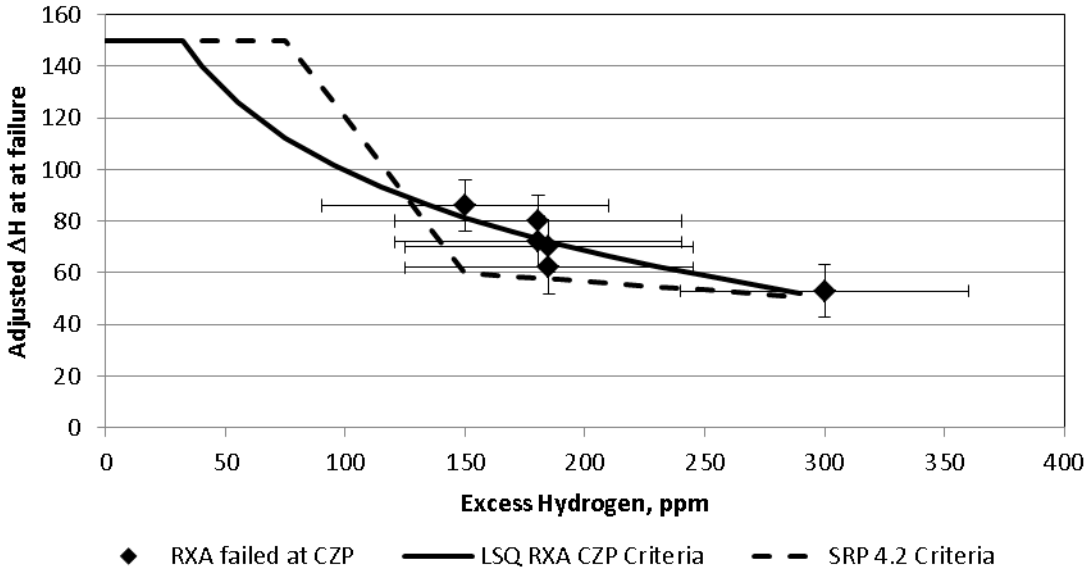

Figure 4.5. Comparison of Least Squares RXA Fit to SRP BWR (RXA) Threshold for CZP with RXA Data at CZP with Error Bars for Uncertainty in Data

The BWR RXA failure threshold from the SRP for PCMI and CZP was provided in terms of excess hydrogen unlike the PWR CWSRA threshold curve from the SRP (in terms of the ratio of oxide-to-cladding wall thickness) such that no calculation is necessary for excess hydrogen. This comparison demonstrates a lower (more conservative) failure threshold for the LSQ fit than the SRP at CZP between 35 and 120 wppm. Between 130 and 270 wppm the SRP threshold is lower (more conservative) with the two approximately the same between 270 and 300 wppm. It should be noted that the shape of the failure threshold curve between 32 wppm and 150 wppm excess hydrogen is speculative because no data exist in this range.

It is further noted that the RXA failed database is very small with only 6 data above 100 wppm where PCMI is the failure mechanism. Therefore, the PCMI failure threshold has a large uncertainty for RXA. High burnup BWR fuel with Zry-2 RXA cladding and burnups above approximately 50 GWd/MTU will have hydrogen levels above 150 wppm with a range up to 350 wppm at 62 GWd/MTU rod average burnup. In addition, no mechanical test data are currently available in the open literature from irradiated Zry-2 RXA cladding with excess hydrogen levels between 100 wppm and 500 wppm to establish a strain level for failure such that FRAPTRAN 1.4 analyses cannot be performed reliably in this hydrogen range. Because of the small RXA failed database, the SRP curve was drawn to bound all of the RXA data that failed because of PCMI.

4.4 Development of the BWR CZP PCMI Failure Threshold for CWSRA Cladding

There are no known experimental data available on RIA behavior from BWR CWSRA cladding. Therefore, it is determined that both the LSQ and SRP PWR failure thresholds for HZP for CWSRA be adjusted down by 18 cal/g (observed PCMI failure threshold difference between hot and cold conditions) and be used as the BWR CZP PCMI failure threshold for CWSRA cladding. The LSQ failure threshold for CWRSA cladding for CZP is given by:

$$\Delta H_{fail} = 327 - 42.3\ln\left(H_{ex}\right) \tag{13}$$

where ΔH_{fail} = enthalpy increase from zero power conditions at failure, cal/g
H_{ex} = cladding excess hydrogen, wppm.

This LSQ fit has a standard deviation of 16.9 cal/g, relative to the data. The maximum enthalpy failure threshold increase at low hydrogen <100 wppm (failure mechanism is ballooning and rupture) is assumed to be 150 cal/g, which is also assumed in the Appendix B of SRP 4.2 (NRC 2007)for BWRs from CZP. The LSQ failure threshold curve intersects the 150 cal/g threshold at approximately 66 wppm excess hydrogen. Therefore the LSQ failure threshold for CSWRA cladding for CZP is given by:

$$\begin{aligned} \Delta H_{fail} &= 150 && H_{ex} \le 66\,ppm \\ \Delta H_{fail} &= 327 - 42.3\ln\left(H_{ex}\right) && H_{ex} > 66\,ppm \le 800\,wppm \end{aligned} \tag{14}$$

A comparison of the LSQ and SRP failure thresholds is provided in Figure 4.6 along with the CABRI and NSRR RIA test data adjusted for CZP. Also, included in Figure 4.6 are error bars (one standard deviation) on the delta failure enthalpy and excess hydrogen of the data. The uncertainties (error bars) for test rodlets not adjusted for hot-to-cold conditions (rodlets tested at CZP are discussed in Section 2.1). Those test rodlets that are adjusted for hot-to-cold conditions (rodlets tested at HZP) have a higher uncertainty on failure enthalpy increase of ± 14 cal/g as discussed in Section 3.3. The limits or excess hydrogen assumes that there is no difference between Zr-4CWSRA and Zr-2CWSRA cladding because this equation is based on Zr-4CWSRA data.

The LSQ fit decreases at a lower excess hydrogen level than the SRP (66 wppm versus 200 wppm in Figure 4.6) providing a lower failure enthalpy between 100 wppm and 300 wppm while above 300 wppm to 600 wppm the SRP failure threshold becomes lower with the two asymptoting to the same failure threshold beyond 600 wppm. The biggest differences between the least squares fit and the SRP are at 200 wppm (103 cal/g versus 150 cal/g), a 47-cal/g difference and at 359 wppm (78 cal/g versus 57 cal/g), a 21-cal/g difference. It is difficult to determine whether the LSQ or SRP curve provides the better fit at low excess hydrogen levels (< 200 wppm) because only one failed point exists. The LSQ failure threshold provides a slightly better fit above 300 wppm excess hydrogen. The SRP BWR failure threshold for CWSRA at CZP (adjusted for hot-to-cold effect of 18 cal/g) is expressed by the following relationships:

$$\begin{aligned}
\Delta H_{fail} &= 150 && H_{ex} \le 180\,ppm \\
\Delta H_{fail} &= 150 - 0.5196\left(H_{ex} - 180\right) && 180\,ppm < H_{ex} \le 359\,ppm \\
\Delta H_{fail} &= 57 - 0.02785\left(H_{ex} - 359\right) && 359\,ppm < H_{ex} \le 800\,ppm
\end{aligned} \tag{15}$$

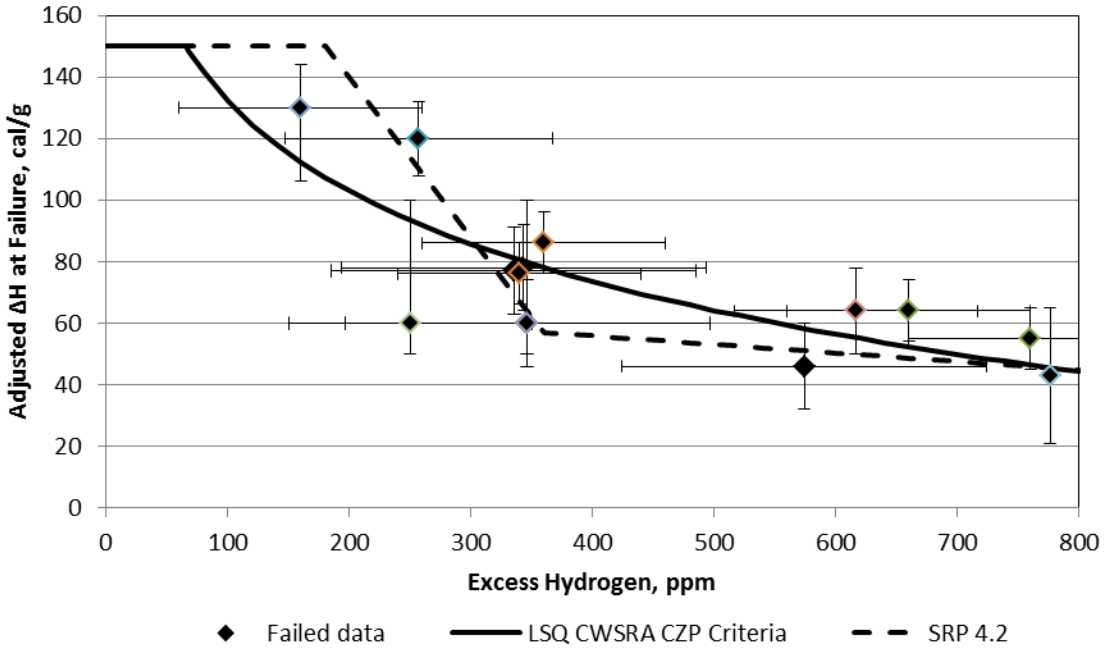

Figure 4.6. Comparison of Least Squares CWSRA Fit to SRP CWSRA Threshold for CZP with CWSRA Data at CZP (hot data adjusted down by 18 cal/g) with Error Bars for Uncertainty in Data

It is acknowledged that the NRC may approve new cladding alloys for BWR operation. For these new cladding alloys, the applicant should either derive a new correlation based on RIA test data with the new alloy, or present data on irradiated cladding that show that the hydride morphology in the new alloy is similar to one of the alloys described above and demonstrate similar mechanical properties including uniform strains at failure that have been proven to be applicable to a RIA event.

4.5 Uncertainty in BWR Failure Thresholds

The uncertainty in the PCMI failure threshold for CWSRA cladding is greatest below 300 wppm of excess hydrogen because only three data points exist by PCMI failure and there is additional uncertainty in one of these three data, the TK2 failure threshold may be higher as discussed in Sections 2.1 and 3.10. In addition, the failure threshold is not valid above 800 wppm excess hydrogen because no failure data exist above this excess hydrogen level for CWSRA cladding.

The uncertainty in the PCMI failure threshold for RXA cladding is the least between 150 wppm and 200 wppm of excess hydrogen because five of the six PCMI failure data exist in this range. As the failure threshold deviates from this range, the uncertainty becomes greater below 150 wppm and between 200 wppm and 300 wppm of excess hydrogen, and is not valid above 300 wppm because of the lack of data.

4.6 Limitations in BWR CZP Failure Threshold

The limitations for application of the BWR Zry-2 CZP failure thresholds

- are BWR fuel designs with gap-to-fuel rod diameter ratio (g/d) limited to 0.0176 or larger (impacts threshold prior to hard gap closure at low-to-moderate burnup levels)
- are applicable to Zry-2 RXA and CWSRA cladding
- are not valid for excess hydrogen above 800 wppm for CWSRA cladding or above 300 wppm of excess hydrogen for RXA cladding because of the lack of data.
- include a burnup limit of 70 GWd/MTU peak pellet (based on data)
- include no fuel additives other than Gd_2O_3, PuO_2, and sintering aids
- are valid for alloys with orientation and distribution of hydrides that are similar to Zry-2 RXA or CWSRA. Mechanical properties must also be similar to one of these alloys.

5.0 Recommended PCMI Failure Thresholds

PNNL recommends the use of the LSQ threshold curves because it provides a better fit to the data where the majority of the data exist; and for RXA (both at HZP and CZP) and for CWSRA (at CZP) is more conservative than the SRP threshold curves where there is no or little data. For CWSRA at HZP and CZP conditions, the greater uncertainty exists between 50 wppm and 200 wppm excess hydrogen because only one PCMI RIA test datum exists in this hydrogen range while 10 RIA test data exist between 300 and 800 wppm. As demonstrated in Figure 4.6, the LSQ threshold for CWSRA cladding under CZP conditions provides the lower (more conservative) PCMI failure threshold between 50 to 250 wppm. The SRP thresholds for CWSRA cladding conservatively bounds the majority of data above 300 wppm; however, this is where the greatest amount of data exists and, therefore, has lower uncertainty in the threshold.

For RXA cladding at HZP and CZP conditions the greater uncertainty exists between 35 and 135 wppm because no PCMI RIA test data exist in this hydrogen range while six data exist between 150 and 300 wppm. As demonstrated in Figures 3.21 and 4.5, the LSQ threshold for RXA cladding under HZP and CZP conditions provides the lower (more conservative) PCMI failure threshold where no data exist between 35 and 135 wppm. The SRP thresholds are more conservative between 150 and 270 wppm; however, this is where the greatest amount data exists and, therefore, has lower uncertainty in the threshold.

The following sections summarize the recommended LSQ failure thresholds.

5.1 LSQ RIA Failure Thresholds for PWR HZP for CWSRA and RXA Cladding

The derived LSQ RIA failure thresholds are summarized below for PWR (HZP) and BWR (CZP) conditions. Figure 5.1 shows the correlations for PWR (HZP) and Figure 5.2 shows the correlations for BWR (CZP).

Stress relief annealed cladding (Zircaloy-4, ZIRLO™)

$$\Delta H_{fail} = 150 \qquad H_{ex} \le 100 wppm$$
$$\Delta H_{fail} = 345 - 42.3\ln(H_{ex}) \qquad 100 wppm < H_{ex} \le 800 wppm$$

Fully recrystallized (M5™)

$$\Delta H_{fail} = 150 \qquad H_{ex} \le 48 wppm$$
$$\Delta H_{fail} = 323 - 44.2\ln(H_{ex}) \qquad 48 wppm < H_{ex} \le 300 wppm$$

where ΔH_{fail} = enthalpy increases from zero power conditions at failure, cal/g
H_{ex} = cladding excess hydrogen, wppm

Other new cladding alloys and partially recrystallized cladding
(e.g., Optimized ZIRLO™)

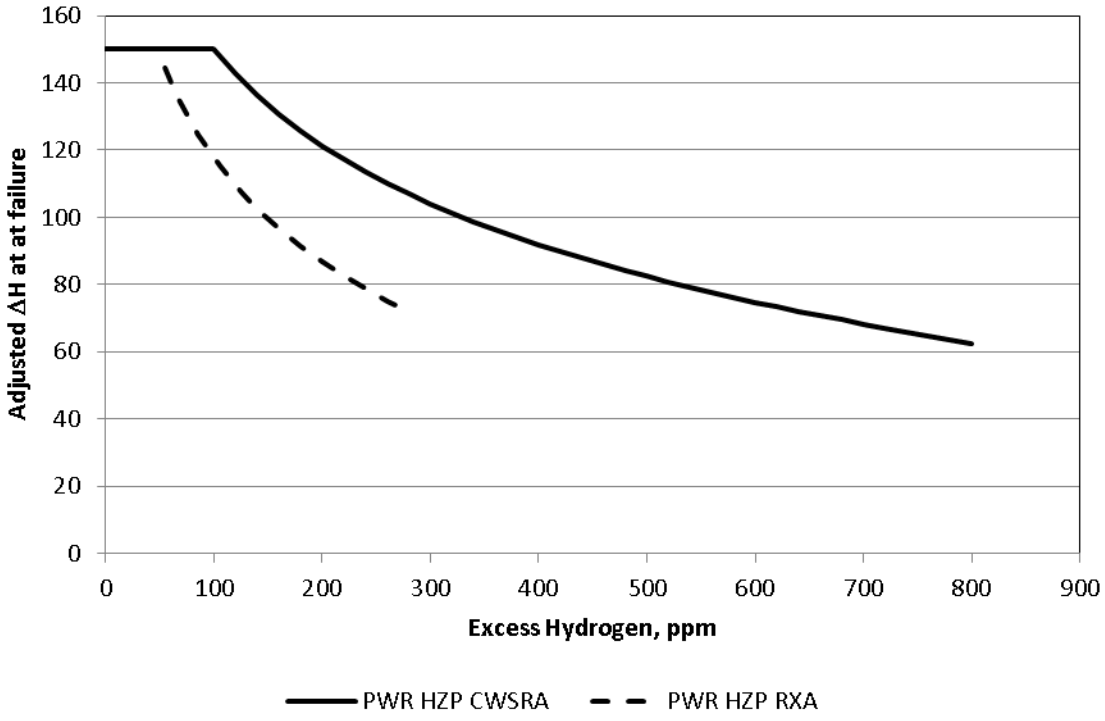

Figure 5.1. Derived LSQ PWR (HZP) Correlations for CWSRA and RXA Cladding Alloys

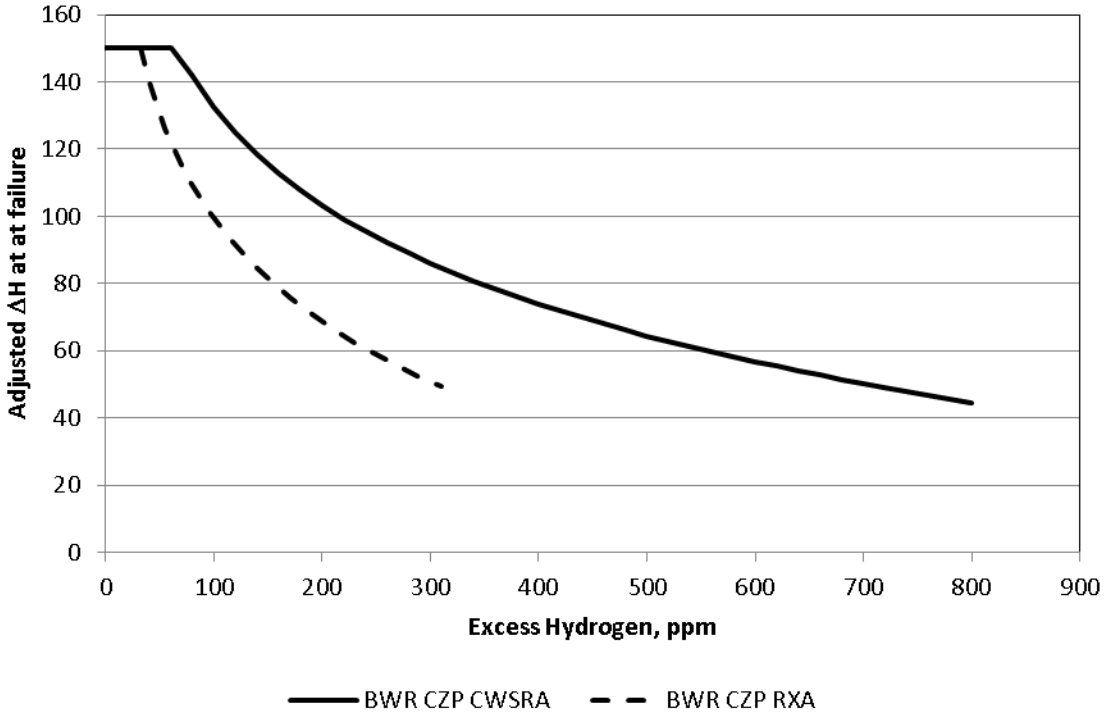

Figure 5.2. Derived LSQ BWR (CZP) Correlations for CWSRA and RXA Cladding Alloys

The licensee is responsible for developing criteria, or the vendor can provide data from irradiated cladding to demonstrate that hydride morphology (orientation and distribution) and mechanical properties of irradiated cladding are the same as one of the above alloys. If the distribution or orientation in the new alloy is different from the alloys tested to date, this cladding would have to be tested at service conditions (in-reactor or out-of-reactor mechanical tests) similar to those for a RIA event to determine a new threshold.

5.2 LSQ RIA Failure Thresholds for BWR CZP for RXA and CWSRA Cladding

Fully recrystallized cladding (Zircaloy-2)

$$\Delta H_{fail} = 150 \qquad H_{ex} \le 32 wppm$$
$$\Delta H_{fail} = 303 - 44.2 \ln(H_{ex}) \qquad 32 wppm < H_{ex} \le 300 wppm$$

Stress relief annealed cladding (Zircaloy-2)

$$\Delta H_{fail} = 150 \qquad H_{ex} \le 66 wppm$$
$$\Delta H_{fail} = 327 - 42.3 \ln(H_{ex}) \qquad 66 wppm < H_{ex} \le 800 wppm$$

where ΔH_{fail} = enthalpy increase from zero power conditions at failure, cal/g
H_{ex} = cladding excess hydrogen, wppm

Other new cladding alloys
(e.g., ZIRON™)

The licensee is responsible for developing criteria, or the vendor can provide data from irradiated cladding to demonstrate that hydride morphology (orientation and distribution) and mechanical properties of irradiated cladding are the same as one of the above alloys using acceptable mechanical test methods demonstrated to be applicable to those conditions for a RIA event. The mechanical test methodology used to measure mechanical properties should demonstrate that it is applicable to failure strains from the CABRI and NSRR tests. If the mechanical properties are reduced (e.g., uniform strain at failure) from the alloys tested to date, this cladding would have to be tested in-reactor or out-of reactor at service conditions similar to those for a RIA event to determine a new threshold.

5.3 Uncertainty in RIA Failure Thresholds

The uncertainty in the BWR and PWR PCMI failure thresholds for CWSRA cladding is greatest below 300 wppm of excess hydrogen because only three data points exist by PCMI failure. In addition, the failure threshold is not valid above 800 wppm excess hydrogen because no failure data exists above this excess hydrogen level.

The uncertainty in the PWR and BWR PCMI failure thresholds for RXA cladding is the least between 150 and 200 wppm of excess hydrogen because five of the six PCMI failure data exist in this range. As the failure threshold deviates from this range, the uncertainty becomes greater below 135 wppm and

between 200 and 300 wppm of excess hydrogen, and is not valid above 300 wppm because of the lack of data.

Because there were only two cold/hot data pairs to base the cold-to-hot adjustment for the PWR HZP thresholds and the hot–to-cold adjustment for the BWR CZP thresholds for CWSRA and RXA cladding, there is a significant uncertainty in this adjustment that is estimated to be ± 14 cal/g.

5.4 Limitations of RIA Failure Thresholds

The following limitations should be applied to either set of the two RIA failure thresholds:

- PWR and BWR fuel designs have a gap–to-fuel rod diameter ratio (g/d) limited to 0.0176 or larger. (This affects the threshold prior to hard gap closure at low-to-moderate burnup levels.)
- BWR failure thresholds are applicable to Zircaloy-2 RXA and CWSRA cladding.
- PWR failure thresholds are applicable to Zircaloy-4 CWSRA, ZIRLO™ CWRA, and M5™ RXA cladding.
- Failure thresholds for CWSRA cladding are not valid for excess hydrogen above 800 wppm, and failure thresholds for RXA cladding are not valid above 300 wppm of excess hydrogen because of the lack of data.
- The burnup limit is 70 GWd/MTU peak pellet.
- No fuel additives other than Gd_2O_3, PuO_2, and sintering aids.
- These limitations are valid for alloys with orientation and distribution of hydrides that are similar to one of the alloys discussed in second and third limitations. Mechanical properties must also be similar to or bounded by one of these alloys.

6.0 References

Alvis J, W Liu, and R Montgomery. 2010. *Fuel Reliability Program: Proposed RIA Acceptance Criteria*. 1021036, Electric Power Research Institute, Palo Alto, California.

Duc B, C Hee, JC Giacalone, and B Siri. 2003a. *Quick Look report of the CIP0-2 test.,* CABRI/WL 2003/40, Institut de Radioprotection et de Sûreté Nucléaire (IRSN), Fontenay-aux-Roses, France.

Duc B, C Hee, JC Giacalone, and J Guilloti. 2003b. *Analysis report of the CABRI CIP0-2 test*. CABRI/WL 2003/52, Institut de Radioprotection et de Sûreté Nucléaire (IRSN), Fontenay-aux-Roses, France.

Federichi E, F Lamare, V Bessiron, and J Papin. 2000. "Status of Development of the SCANAIR Code for the Description Of Fuel Behavior Under Reactivity Initiated Accident (RIA)," *ANS International Topical Meeting on LWR Fuel Performance,* April 10-13, Park City, Utah.

Fuketa T, H Sasajima, Y Tsuchiuchi, Y Mori, T Nakamura, and K. Ishijima. 1997. "NSRR/RIA Experiments with High Burnup PWR Fuels," In *Proceedings of the 1997 International Topical Meeting on LWR Fuel Performance, Portland, Oregon, March 2-6, 1997*. American Nuclear Society, La Grange Park, Illinois.

Fuketa T, H Sasajima, and T Sugiyama. 2001. "Behavior of High-Burnup PWR Fuels with Low-Tin Zircaloy-4 Cladding Under Reactivity-Initiated-Accident Conditions," *Nuclear Technology* 133:50-62.

Fuketa T, T Sugiyama, and F Nagase. 2006a. "Behavior of 60 to 78 MWd/kgU PWR fuels under reactivity-initiated accident conditions," *Journal of Nuclear Science and Technology* 43(9):1080–1088.

Fuketa T, T Sugiyama, M Umeda, K Tomiyasu, and H. Sasajima. 2006b. "Behaviour of high burnup PWR fuels during simulated reactivity-initiated accident conditions." *TopFuel 2006 Transactions, Salamanca, Spain. October 22–26, 2006,* pp.279-283. European Nuclear Society.

Fuketa T, T Sugiyama, M Umeda, H Sasajima, and F Nagase. 2009. "Behavior of LWR/MOX Fuels under Reactivity-Initiated Accident Conditions." In *Water Reactor Fuel Performance Meeting 2009, TopFuel 2009 Paris, France 6-10 September 2009.* pp. 465-472. Societe Francaise D'Energie Nucleaire, Paris, France.

Geelhood KJ and CE Beyer. 2011. "Hydrogen Pickup Models for Zircaloy-2, Zircaloy-4, M5™ and ZIRLO™." Water Reactor Fuel Performance Meeting, Chengdu, China, September 11-14, 2011. Accessed on April 15, 2013 at http://pbadupws.nrc.gov/docs/ML1209/ML12093A469.pdf.

Geelhood KJ, CE Beyer, and WG Luscher. 2008. *PNNL Stress/Strain Correlation for Zircaloy*. PNNL-17700, Pacific Northwest National Laboratory Richland, Washington.

Geelhood KJ, WG Luscher, and CE Beyer. 2010. *FRAPCON-3.4: A Computer Code for the Calculation of Steady-State, Thermal-Mechanical Behavior of Oxide Fuel Rods for High Burnup*, NUREG/CR-7022, Vol. 1 (PNNL-19418, Vol. 1), Pacific Northwest National Laboratory Richland, Washington.

Geelhood KJ, WG Luscher, CE Beyer, and JM Cuta. 2011. *FRAPTRAN 1.4: A Computer Code for the Transient Analysis of Oxide Fuel Rods*, NUREG/CR-7023, Vol. 1, PNNL-19400, Vol. 1, Pacific Northwest National Laboratory, Richland, Washington.

Georgenthum V. 2009. "Influence of test conditions on the PCMI behaviour during RIA based on CIP0-1, VA-1 and VA-3 tests," Fuel Safety Research Meeting, Tokai Mura, Japan, May 20 and 21, 2009.

Jeury F, C Hee, JC Giacalone, and B Siri. 2003. *Quick Look report of the CIP0-1 test*. CABRI/WL 2003/41, Institut de Radioprotection et de Sûreté Nucléaire (IRSN), Fontenay-aux-Roses, France.

Jeury F, C Hee, JC Giacalone, and J Guillot. 2004. *Analysis report of the CABRI CIP0-1 test*. CABRI/WL 2004/55, Institut de Radioprotection et de Sûreté Nucléaire (IRSN), Fontenay-aux-Roses, France.

Kearns JJ. 1967. "Thermal Solubility and Partitioning of Hydrides in the Alpha Phase of Zirconium, Zircaloy-2 and Zircaloy-4." *Journal of Nuclear Materials* 22:292–303.

Kubo T, K Sakamoto, and T Higuchi. 2010. "Fracture Strength of Zirconium Hydrides Embedded in a Zircaloy-2 Matrix And Its Effects on the Initiation of Delayed Hydride Cracking." In *Proceedings of 2010 LWR Fuel Performance/TopFuel/WRFPM*, Orlando, Florida, September 26-29.

Nakamura T, M Yoshinaga, MM Sobajima, K Ishijima, and T Fujishiro. 1994. "Boiling Water Reactor Fuel Behavior at Burnup of 26 GWd/tonne U Under Reactivity-Initiated-Accident Conditions." *Nuclear Technology*, 108:45-59.

Nakamura T, T Fuketa, T Sugiyama, and S Sasajima. 2004. "Failure Thresholds of High Burnup BWR Fuel Rods under RIA Conditions." *Journal of Nuclear Science and Technology* 41(1)37-43.

NEA. 2010. *Nuclear Fuel Behavior Under Reactivity-Initiated Accident (RIA) Conditions- State of the Art Report*. NEA/CSNI/R(2010) Nuclear Energy Agency, Organisation for Economic Co-operation and Development, Paris, France.

NRC – U.S. Nuclear Regulatory Commission. 1974. *Assumptions Used for Evaluating a Control Rod Ejection Accident for Pressurized Water Reactors*. Regulatory Guide 1.77. U.S. Nuclear Regulatory Commission, Washington D.C.

NRC – U.S. Nuclear Regulatory Commission. 2004. "An Assessment of Postulated Reactivity-Initiated Accidents (RIAs) for Operating Reactors in the U.S." Research Information Letter No. 0401 in the U.S. Nuclear Regulatory Commission Library, ADAMS ML040920189.

NRC – U.S. Nuclear Regulatory Commission. 2007. "Fuel System Design," Chapter 4, Section 4.2, Revision 3 of *Standard Review Plan for the Review of Safety Analysis Reports for Nuclear Power Plants LWR Edition—Reactor*. NUREG-0800. U.S. Nuclear Regulatory Commission, Washington D.C.

Papin J, B Cazalis, JM Frizonnet, E Fédérici, and F Lemoine. 2003. "Synthesis of Cabri-RIA Tests Interpretation," The Eurosafe Forum 2003, Paris, France, November 25 and 26. Accessed April 15, 2013 at http://pbadupws.nrc.gov/docs/ML0402/ML040220024.pdf.

Papin J, B Cazalis, JM Frizonnet, E Fédérici, J Desquines, F Lemoine, V Georgenthum, F Lamare, and M Metit. 2007. "Summary and Interpretation of the Cabri REP-Na Program." *Nuclear Technology* 157(3):230-250.

Petit, M, V Georgenthum, T Sugiyama, M Quecedo, and J Desquines. 2007. "A Comparative analysis of CABRI CIPO-1 and NSRR VA-2 Reactivity Initiated Accident Tests." *Proceedings of EUROSAFE Forum - Securing Nuclear Safety in Future Years, November 5 and 6, 2007, Berlin, Germany*.

Sugiyama T, M Umeda, H Sasajima, M Suzuki, and T Fuketa. 2009a. "Effect of Initial Coolant Temperature on Mechanical Fuel Failure under Reactivity-Initiated Accident Conditions." In *Water Reactor Fuel Performance Meeting 2009, TopFuel 2009 Paris, France 6-10 September 2009.* pp. 489-496. Societe Francaise D'Energie Nucleaire, Paris, France.

Sugiyama T, M Umeda, Y Udagawa, H Sasajima, M Suzuki, and T Fuketa. 2009b. "Applicability of NSRR Room/High Temperature Test Results to fuel Safety Evaluation under Power Reactor Conditions." In *Nuclear Fuel Behaviour during Reactivity Initiated Accidents Workshop Proceedings, September 9–11, 2009.* NEA/CSNI/R(2010)7, Organisation for Economic Co-operation and Development, Nuclear Energy Agency, Paris, France.

Sugiyama T, Y Udagawa, M Suzuki, and F Nagase. 2011. "Influence of Coolant Temperature and Power Pulse Width on Fuel Failure Limit under Reactivity Initiated Accident Conditions." In *Proceedings of Water Reactor Fuel Performance Meeting/LWR/Top Fuel, Chengdu, China, September 11-14, 2011*.

Suzuki M, T Sugiyama, Y Udagawa, F Nagase, and T Fuketa. 2009. "Numerical Analysis and Simulation of Behavior of High Burnup PWR Fuel Pulse-Irradiated in Reactivity-Initiated Accident Conditions." *Nuclear Fuel Behaviour during Reactivity Initiated Accidents Workshop Proceedings, September 9–11, 2009.* NEA/CSNI/R(2010)7, Organisation for Economic Co-operation and Development, Nuclear Energy Agency, Paris, France.

Udagawa Y, T Sugiyama, M Suzuki, and F Nagase. 2011. "PCMI Failure Limit Assessed by Fracture Mechanics Approach Based on NSRR High-Burnup PWR Fuel Tests." In *Proceedings of the International Atomic Energy Agency Meeting on Fuel Behavior and Modeling Under Severe Transient and LOCA Conditions*, October 18 – 21, 2011, Mito-city Ibaraki-ken, Japan.

Vitanza C and JM Conde-Lopez. 2004. "PCMI Implications of High Burn-up Light Water Reactor Fuel In reactivity-Initiated Accidents." In *Pellet-Clad Interaction in Water Reactor Fuels Seminar Proceedings* (PCI-2004), Aix-en-Provence, France, March 9 -11, 2004, Organisation for Economic Co-operation and Development, Nuclear Energy Agency, Paris, France.

Vitanza C and M Hrehor. 2006. *Review of High Burnup RIA and LOCA Database and Criteria*. Report NEA/CSNI/R(2006)5, Organisation for Economic Co-operation and Development, Nuclear Energy Agency, Committee on the Safety of Nuclear Installations, Paris, France.

Yegorova L, K Lioutov, N Jouravkova, O Nechaeva, A Salatov, V Smirnov, A Goryachev, V Ustinenko, and I Smirnov. 2005a. *Experimental Study of Narrow Pulse Effects on the Behavior of High Burnup Fuel Rods with Zr-1%Nb Cladding and UO_2 Fuel (VVER Type) under Reactivity-Initiated Accident Conditions: Program Approach and Analysis of Results*. NUREG/IA-0213, Vol. 1, Nuclear Safety Institute of Russian Research Center "Kurchatov Institute," Moscow, Russia.

Yegorova L, K Lioutov, N Jouravkova, O Nechaeva, A Salatov, V Smirnov, A Goryachev, V Ustinenko, and I Smirnov. 2005b. *Experimental Study of Narrow Pulse Effects on the Behavior of High Burnup Fuel Rods with Zr-1%Nb Cladding and UO_2 Fuel (VVER Type) under Reactivity-Initiated Accident Conditions: Test Conditions and Results*. NUREG/IA-0213, Vol. 2, Nuclear Safety Institute of Russian Research Center "Kurchatov Institute," Moscow, Russia.

Appendix A
Pressurized Water Reactor Test Rod Results from CABRI and Nuclear Safety Research Reactor

Appendix A
Pressurized Water Reactor Test Rod Results from CABRI and Nuclear Safety Research Reactor

Table A.1 presents the latest published data for each of these rodlet tests, these may be different from earlier published values, it is assumed that the latest published values represent the best values. In most cases the total hydrogen level in Table A.1 are based on calculated values that are noted with an asterisk, these values are calculated from the pickup fractions given in Section 3.0 of this report and the average of the range of oxide thicknesses measured for the test rodlet. The following is a brief discussion of the uncertainty in the peak fuel enthalpy and the total hydrogen level.

The peak fuel enthalpy change at failure is calculated with a fuel performance code such as fuel rod analysis program transient (FRAPTRAN)-1.4 (Geelhood et al. 2011) or SCANAIR (Federichi et al. 2000) that uses the input of total energy deposited measured during the pulse period and the time of failure as determined from the microphone signal. The uncertainty in the total energy deposited is approximately 7 percent while the uncertainty in the code-calculated delta energy increase at failure is approximately 10 percent (includes uncertainty in timing of failure and code calculation).

The uncertainty in the hydrogen measurement is difficult because in most cases it is usually measured on the father rod at an axial position near where the rodlet was cut. The measurement is usually performed on a full circumference ring of cladding. It is known that hydrogen can vary considerably both circumferentially and axially because it diffuses to cold regions in the cladding such that it does not always remain where it originated. Therefore, there is an uncertainty in the hydrogen measurement because the measurement was not performed at the axial location where failure in the rodlet was experienced. The uncertainty (standard deviation) in the measured hydrogen levels is assumed to be 23 percent (above 25 μm oxide thickness) for Zry-4 and ZIRLO™ (CWSRA) and 29 percent for M5 (RXA) that are based on a statistical evaluation of measured oxide thicknesses and hydrogen measurements (see Section 2.1). Therefore, uncertainty in predicted hydrogen from oxide thickness includes uncertainty in the measurement plus the uncertainty in the hydrogen pickup fractions.

The uncertainty in measured and predicted hydrogen for the boiling water reactor (BWR) Zr-2 RXA cladding is assumed to be 60 wppm absolute uncertainty. The BWR (Zr-2 RXA) hydrogen uncertainties in predicted values were based on an evaluation by Geelhood and Beyer (2010).

Table A.1. PWR CABRI and Nuclear Safety Research Reactor Test Rod Results

Reactor/Test	Failure/non-failure	Enthalpy Increase Reported at Failure (Maximum)	Fuel Type	Cladding Type	Oxide Thickness, microns	Total Hydrogen level, wppm	Excess Hydrogen wppm
SODIUM LOOP PWR TESTS							
CABRI/Na1[1,2]	Failure	13(97)	UO_2	Zry-4 CWSRA	80 - 100	702*	652
CABRI/Na2[1,2]	non-failure	182	UO_2	Zry-4 CWSRA	10	71*	21
CABRI/Na3[1,2]	non-failure	107	UO_2	Zry-4 CWSRA	35 - 60	371*	321
CABRI/Na4[1,2]	non-failure	68	UO_2	Zry-4 CWSRA	60 - 80	546*	496
CABRI/Na5[1,2]	non-failure	91	UO_2	Zry-4 CWSRA	15 - 25	156*	106
CABRI/Na6[1,2]	non-failure	116	MOX	Zry-4 CWSRA	35	275*	225
CABRI/Na7[1,2]	Failure at 0.405 sec	96(121)	MOX	Zry-4 CWSRA	50	393*	343
CABRI/Na8[1,2]	Failure at 0.5318 sec	44 - 78(81)	UO_2	Zry-4 CWSRA	84 - 126	826*	776
CABRI/Na9[1,2]	non-failure	180	MOX	Zry-4 CWSRA	10	79*	29
CABRI/Na10[1,2]	Failure	64(81)	UO_2	Zry-4 CWSRA	60 - 100	624*	574
CABRI/Na11[2]	non-failure	75	UO_2	M5	15 - 20	65 - 70	18
CABRI/Na12[2]	non-failure	86	MOX	Zry-4 CWSRA	59 - 72	515*	465
CABRI/CIPO1[3,4,5]	non-failure	74	UO_2	ZIRLO™	75 - 85	800	750
CABRI/CIPO2[12,13]	non-failure	64	UO_2	M5	20 - 25	70 - 92	31
COLD CAPSULE PWR TESTS							
NSRR/TK1[6]	non-failure	126	UO_2	Zry-4 CWSRA	7	55*	55
NSRR/TK2[6]	Failure	60 (107)	UO_2	Zry-4 CWSRA	15-35	250	250
NSRR/TK3[6]	non-failure	99	UO_2	Zry-4 CWSRA	4-12	85*	85
NSRR/TK4[6]	non-failure	98	UO_2	Zry-4 CWSRA	25	197*	197
NSRR/TK5[6]	non-failure	101	UO_2	Zry-4 CWSRA	30	236*	236
NSRR/TK6[6]	non-failure	125	UO_2	Zry-4 CWSRA	15	118*	118
NSRR/TK7[6]	Failure	86 (95)	UO_2	Zry-4 CWSRA	30	360	360

Reactor/Test	Failure/non-failure	Enthalpy Increase Reported at Failure (Maximum)	Fuel Type	Cladding Type	Oxide Thickness, microns	Total Hydrogen level, wppm	Excess Hydrogen wppm
NSRR/HBO1[6]	Failure	60 (73)	UO_2	Zry-4 CWSRA	40-48	378*	378
NSRR/HBO2[6]	non-failure	37	UO_2	Zry-4 CWSRA	30-40	315*	315
NSRR/HBO3[6]	non-failure	74	UO_2	Zry-4 CWSRA	20-25	197*	197
NSRR/HBO4[6]	non-failure	50	UO_2	Zry-4 CWSRA	15-20	157*	157
NSRR/HBO5[6]	Failure	77 (80)	UO_2	Zry-4 CWSRA	35-60	424*	424
NSRR/HBO6[6]	non-failure	85	UO_2	Zry-4 CWSRA	20-30	212*	212
NSRR/HBO7[6]	non-failure	88	UO_2	Zry-4 CWSRA	35-45	318*	318
NSRR/OI1[7]	non-failure	106	UO_2	Zry-4 CWSRA	15	106*	106
NSRR/OI2[7]	non-failure	108	UO_2	Zry-4 CWSRA	15	106*	106
NSRR/OI10[8]	non-failure	104	UO_2	MDA	27	248*	248
NSRR/OI11[8]	Failure	120 (157)	UO_2	ZIRLO™	28	257*	257
NSRR/OI12[8]	non-failure	143	UO_2	NDA	41	290*	290
NSRR/MH1[7]	non-failure	47	UO_2	Zry-4 CWSRA	4	29*	29
NSRR/MH2[7]	non-failure	55	UO_2	Zry-4 CWSRA	4	29*	29
NSRR/MH3[7]	non-failure	67	UO_2	Zry-4 CWSRA	4	29*	29
NSRR/GK1[7]	non-failure	93	UO_2	Zry-4 CWSRA	10	72*	72
NSRR/GK2[7]	non-failure	90	UO_2	Zry-4 CWSRA	10	72*	72
NSRR/VA1[9]	Failure	64 (133)	UO_2	ZIRLO™	73	660	660
NSRR/VA2[9]	Failure	55 (130)	UO_2	MDA	70	760	760
NSRR/RH1[10]	non-failure	110	UO_2	M5	6	70	70
NSRR/BZ1[11]	Failure	76(164)	MOX	Zry-4 CWSRA	30	340	340
NSRR/BZ2[11]	Failure	130 (154)	MOX	Zry-4 CWSRA	20	160	160
NSRR/MR-1[10]	non-failure	97	UO_2	NDA	39	210	210

Reactor/Test	Failure/non-failure	Enthalpy Increase Reported at Failure (Maximum)	Fuel Type	Cladding Type	Oxide Thickness, microns	Total Hydrogen level, wppm	Excess Hydrogen wppm
HOT CAPSULE PWR TESTS							
NSRR/VA3[9]	Failure	82 (108)	UO_2	ZIRLO™	82	670	617
NSRR/VA4[9]	non-failure	109	UO_2	MDA	80	760	707
NSRR/RH2[14]	non-failure	90	UO_2	M5	6	69 - 70	17
NSRR/BZ3[11]	non-failure	126	MOX	Zry-4 CWSRA	20	160	107

CWSRA = cold-worked stress relief annealed
MDA = Mitsubishi Developed Alloy
MOX = mixed uranium and plutonium dioxide
NDA = New Development Alloy
NNAR = Nuclear Safety Research Reactor
PWR = pressurized water reactor
UO_2 = uranium dioxide

*these hydrogen values are calculated by PNNL based on the oxide thickness and alloy

[1](Papin et al. 2003)
[2](Papin et al. 2007)
[3](Georgenthum 2009)
[4](Jeury et al. 2003)
[5](Jeury et al. 2004)
[6](Fuketa et al. 2001)
[7](Fuketa et al. 1997)
[8](Fuketa et al. 2006a)
[9](Sugiyama et al. 2009a)
[10](Fuketa et al. 2006b)
[11](Fuketa et al. 2009)
[12](Duc et al. 2003a)
[13](Duc et al. 2003b)
[14](Sugiyama et al. 2009b)

Appendix B
Boiling Water Reactor Nuclear Safety Research Reactor Test Rod (Zry-2 RXA Cladding) Results

Appendix B - Boiling Water Reactor Nuclear Safety Research Reactor Test Rod (Zry-2 RXA Cladding) Results

Reactor/Test	Failure/non-failure	Enthalpy Increase Reported at Failure (Maximum)	Fuel Type	Cladding Type	Oxide Thickness, microns	Total Hydrogen level, wppm*	Excess Hydrogen wppm
COLD CAPSULE BWR TESTS							
NSRR/FK1[1]	non-failure	130	UO_2	Zry-2 RXA	11	72	72
NSRR/FK2[1]	non-failure	70	UO_2	Zry-2 RXA	11	72	72
NSRR/FK3[1]	non-failure	145	UO_2	Zry-2 RXA	15	72	72
NSRR/FK4[1]	non-failure	140	UO_2	Zry-2 RXA	10	82	82
NSRR/FK5[1]	non-failure	70	UO_2	Zry-2 RXA	10	82	82
NSRR/FK6[1]	Failure	70 (131)	UO_2	Zry-2 RXA	20	150- 220	220
NSRR/FK7[1]	Failure	62 (129)	UO_2	Zry-2 RXA	20	150- 221	221
NSRR/FK8[1]	non-failure	65	UO_2	Zry-2 RXA	20	141-159	159
NSRR/FK9[1]	Failure	86 (90)	UO_2	Zry-2 RXA	20	141-159	159
NSRR/FK10[1]	Failure	80(103)	UO_2	Zry-2 RXA	20	141-220	220
NSRR/FK12[1]	Failure	72(89)	UO_2	Zry-2 RXA	20	141-220	220
NSRR/TS1[2]	non-failure	55	UO_2	Zry-2 RXA	6	54*	54
NSRR/TS2[2]	non-failure	66	UO_2	Zry-2 RXA	6	54*	54
NSRR/TS3[2]	non-failure	88	UO_2	Zry-2 RXA	6	54*	54
NSRR/TS4[2]	non-failure	84	UO_2	Zry-2 RXA	6	54*	54
NSRR/TS5[2]	non-failure	98	UO_2	Zry-2 RXA	6	54*	54
NSRR/LS1[3]	Failure	53 (112)	UO_2	Zry-2 RXA	25	300	300
NSRR/DW-1[4]	non-failure	121	MOX	Zry-2 RXA	10	50	50
HOT CAPSULE TESTS BWR							
NSRR/LS2[3]	non-failure	89	UO_2	Zry-2 RXA	25	290	237

BWR = boiling water reactor
MOX = Mixed uranium and plutonium dioxide
NSRR = Nuclear Safety Research Reactor
RXA = recrystallized annealed
UO_2 = uranium dioxide

*these hydrogen values are calculated by PNNL based on the oxide thickness and alloy

[1](Nakamura et al. 2004)
[2](Nakamura et al. 1994)
[3](Sugiyama 2009a and b)
[4](Fuketa 2009)

Pacific Northwest
NATIONAL LABORATORY

Proudly Operated by **Battelle** *Since 1965*

U.S. DEPARTMENT OF
ENERGY

902 Battelle Boulevard
P.O. Box 999
Richland, WA 99352
1-888-375-PNNL (7665)
www.pnnl.gov